

Journal Pre-proof



Efficient chemical and microbial removal of iron and manganese in a rapid sand filter and impact of regular backwash

Signe Haukelidsaeter, Alje S. Boersma, Lina Piso, Wytze K. Lenstra, Niels A.G.M. van Helmond, Frank Schoonenberg, Erik van der Pol, Luis C.C. Hurtarte, Paul W.J.J. van der Wielen, Thilo Behrends, Maartje A.H.J. van Kessel, Sebastian Lücker, Caroline P. Slomp

PII: S0883-2927(24)00009-X

DOI: <https://doi.org/10.1016/j.apgeochem.2024.105904>

Reference: AG 105904

To appear in: *Applied Geochemistry*

Received Date: 26 July 2023

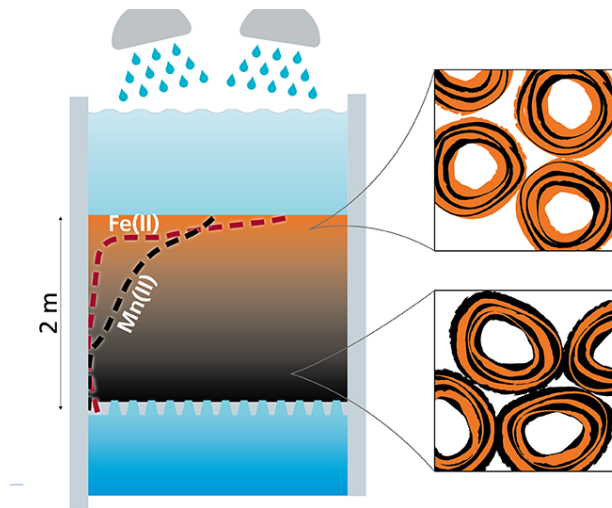
Revised Date: 15 December 2023

Accepted Date: 7 January 2024

Please cite this article as: Haukelidsaeter, S., Boersma, A.S., Piso, L., Lenstra, W.K., van Helmond, N.A.G.M., Schoonenberg, F., van der Pol, E., Hurtarte, L.C.C., van der Wielen, P.W.J.J., Behrends, T., van Kessel, M.A.H.J., Lücker, S., Slomp, C.P., Efficient chemical and microbial removal of iron and manganese in a rapid sand filter and impact of regular backwash, *Applied Geochemistry* (2024), doi: <https://doi.org/10.1016/j.apgeochem.2024.105904>.

This is a PDF file of an article that has undergone enhancements after acceptance, such as the addition of a cover page and metadata, and formatting for readability, but it is not yet the definitive version of record. This version will undergo additional copyediting, typesetting and review before it is published in its final form, but we are providing this version to give early visibility of the article. Please note that, during the production process, errors may be discovered which could affect the content, and all legal disclaimers that apply to the journal pertain.

© 2024 Published by Elsevier Ltd.



- Coatings reflect Fe and Mn removal
- Backwash removes Fe flocs & sustains water flow
- Stratified biological community despite backwash
- Layered coatings indicate full vertical mixing of filter medium after several backwash cycles

Journal Pre-proof

1 Efficient chemical and microbial removal of iron and
2 manganese in a rapid sand filter and impact of regular
3 backwash
4

5 **Signe Haukelidsaeter¹, Alje S. Boersma², Lina Piso^{1,2}, Wytze K. Lenstra^{1,2}, Niels A.G.M. van**
6 **Helmond^{1,2}, Frank Schoonenberg³, Erik van der Pol³, Luis C.C. Hurtarte^{4,5}, Paul W.J.J. van der**
7 **Wielen^{6,7}, Thilo Behrends¹, Maartje A.H.J. van Kessel², Sebastian Lücker², Caroline P. Slomp^{1,2}**

8 ¹ Department of Earth Sciences, Faculty of Geosciences, Utrecht University, P.O Box 80021, 3508 TA
9 Utrecht, the Netherlands

10 ² Department of Microbiology, Radboud Institute of Biological and Environmental Science, Faculty of
11 Science, Radboud University, P.O. Box 9010, 6500 GL Nijmegen, The Netherlands

12 ³ Vitens N.V., P.O. Box 1205, 8001 BE Zwolle, The Netherlands

13 ⁴ European Synchrotron Radiation Facility - 71, avenue des Martyrs, CS 40220, 38043 Grenoble Cedex
14 9, France.

15 ⁵ Diamond Light Source Ltd., Didcot, Oxfordshire OX11 0DE, UK

16 ⁶ KWR Water Research Institute, P.O. Box 1072, 3430 BB Nieuwegein, The Netherlands

17 ⁷ Laboratory of Microbiology, Wageningen University & Research, Stippeneng 4, 6708 WE,
18 Wageningen, The Netherlands

19

20 **ABSTRACT**

21 Aeration followed by rapid sand filtration is a common method in drinking water treatment to remove
22 iron (Fe) and manganese (Mn) from anoxic groundwater. To ensure the successful removal of Fe and
23 Mn within a single filter, several factors such as raw water characteristics, backwash procedures and
24 chemical and microbial interactions with the filter medium need to be considered. Here, we assess the
25 characteristics of a single medium rapid sand filter with highly efficient removal of Fe and Mn. Using
26 synchrotron X-ray spectroscopy, we show that formation of ferrihydrite-type Fe oxides in the top of the
27 filter (0-50 cm) accounts for > 95 % of the removal of dissolved Fe²⁺ in the filter. Birnessite-type Mn-
28 oxides, which are thought to be biogenic, form over a wider depth interval (0-110 cm). Results of 16S
29 rRNA gene amplicon sequencing indicate a corresponding distinct vertical stratification of the microbial
30 community, with potential iron-oxidizing *Gallionella*, *Leptothrix* and *Sideroxydans* dominating in the
31 upper part of the filter, and nitrifiers being more prevalent deeper in the filter. Besides Fe and Mn-oxide,
32 Fe-flocs and bacteriological hollow sheets form in the upper part of the filter. Both the Fe-flocs, hollow
33 Fe-sheets and part of the Fe and Mn coatings are removed through backwashing, thereby reducing the
34 pressure difference measured over the filter medium linked to clogging of pores (from 14 kPa to 1.5
35 kPa) and ensuring continued water flow. Backwashing removes part of the *Gallionella*, but this does
36 not negatively impact the filter performance. Strikingly, SEM imaging with EDS mapping revealed
37 alternating layers of Fe and Mn-oxides on the coated grains throughout the filter. This indicates slow
38 mixing of the filter medium between the upper 30 cm and the rest of the filter during backwashing.
39 Slow mixing likely contributes to continued success of the filter by ensuring homogeneous filter bed
40 growth, while still allowing for stratification of the microbial community.

41 1. INTRODUCTION

42 Groundwater serves as a vital drinking water source globally. Redox-sensitive elements such as iron
43 (Fe) and manganese (Mn) often are present in anoxic groundwater. To ensure the provision of safe
44 water and prevent aesthetic problems and fouling of distribution infrastructure with metal
45 (oxyhydr)oxides (henceforth termed metal-oxides), the removal of these elements is essential (Buamah
46 et al., 2009; Vries et al., 2017). A commonly employed method for removing dissolved Fe^{2+} and Mn^{2+}
47 from anoxic groundwater, without the use of chemical oxidants, involves aeration followed by rapid
48 sand filtration. Despite the widespread use of this technology, the design and operation of sand filters
49 have predominantly relied on empirical knowledge from plant operators accumulating over the years.
50 Consequently, a comprehensive understanding of the characteristics of a well-functioning filter and
51 how removal efficiencies depend on water chemistry, regular backwashing and associated filter medium
52 characteristics is lacking.

53 In sand filters with high oxygen concentrations ($\text{O}_2 > 250 \mu\text{M}$), dissolved Fe^{2+} precipitates with low
54 crystallinity, such as ferrihydrite ($\text{Fe}_{8.2}\text{O}_{8.5}(\text{OH})_4 \cdot 3\text{H}_2\text{O}$; Michel et al., 2010) form in the top of the filter
55 through homogeneous, heterogeneous or biological oxidation (Van Beek et al., 2016). Homogeneous
56 Fe^{2+} oxidation refers to the oxidation of Fe^{2+} by dissolved oxygen and subsequent hydrolysis and
57 precipitation of Fe-flocs. The process is rapid at near-neutral pH and typically occurs already in the
58 supernatant on top of the filter (Gude et al., 2018; Vries et al., 2017). Heterogeneous Fe^{2+} oxidation
59 refers to a series of reactions with oxidation and precipitation following surface adsorption of Fe^{2+}
60 (Tamura et al., 1980; Van Beek et al., 2016). The ferrihydrite formed in sand filters through both
61 pathways is mostly present as globular nodules (diameter of 2-6 nm), characterized by a high degree of
62 surface roughness and a large surface area (Carta et al., 2009; Sharma et al., 2002). Iron-oxidizing
63 bacteria use Fe^{2+} as an electron donor and, thus, can contribute to Fe removal in rapid sand filters as
64 well (de Vet et al., 2011; Gülay et al., 2013). Bacteria belonging to the genera *Gallionella* and
65 *Leptothrix*, for instance, are known iron-oxidizers, and their activity leads to the presence of
66 characteristic twisted stalks and hollow sheets, respectively, that can be detected microscopically (Chan
67 et al., 2010; Krepski et al., 2012). However, some iron-oxidizing *Gallionella* and *Sideroxydans* species

68 can also produce particulate Fe-oxides of an amorphous morphotype (Emerson et al., 2010; Lin et al.,
69 2012).

70 In rapid sand filters, Mn^{2+} is usually removed through heterogeneous and/or biological oxidation. While
71 heterogeneous oxidation leads to the formation of Mn(III) or Mn(III)/Mn(II)-oxides including
72 hausmannite, manganite or feitknechtite (Inoué et al., 2019; Lan et al., 2017; Murray et al., 1985)
73 microbially catalyzed Mn(II) oxidation results in the precipitation of Mn(IV)-phyllophanes such
74 as birnessite or todorokite (Kim et al., 2003; Tebo et al., 2004; Villalobos et al., 2003; Webb et al.,
75 2005). Biological Mn^{2+} oxidation likely plays an important role in the start-up phase of sand filters, but
76 when filters age, it is believed that Mn^{2+} oxidation becomes predominantly heterogeneous (Bruins et
77 al., 2015). Birnessite has a high negative charge and is characterized by a typical coral or sponge-like
78 structure that is visible using an electron microscope (Jiang et al., 2010, Bruins et al., 2015). Microbially
79 produced Mn-oxides cannot easily be distinguished from those formed through chemical oxidation
80 based on imaging. Techniques such as micro-focused Mn K-edge X-ray spectroscopy, however, can be
81 used to provide crucial information to distinguish biologically and chemically formed Mn-oxides by
82 characterizing the redox state and local coordination environment of Mn (Zahoransky et al., 2022).
83 Removal of Mn^{2+} in rapid sand filters can be hindered by high concentrations of Fe^{2+} or ammonium
84 (NH_4^+) in the raw water, possibly due to lowering the contact time with the filter medium, or due to the
85 reductive dissolution of Mn-oxides by Fe^{2+} (Gouzinis et al., 1998; Haukelidsaeter et al., 2023; Tian et
86 al., 2019).

87 Regular backwashing of sand filters is necessary to remove metal-oxides and to restore hydraulic
88 function (Ramsay et al., 2021). The upward flow of water and air leads to mixing of filter medium, with
89 the largest displacement often occurring in the top of the filter (Ramsay et al., 2021). Nevertheless, this
90 mixing may still lead to a homogeneous composition of the filter bed and microbial community
91 composition, as suggested in a recent study (Corbera-Rubio et al., 2023), but whether this holds for
92 rapid sand filters in general remains to be confirmed.

93 In this study, we assessed the chemical and microbiological processes contributing to successful Fe and
94 Mn removal and the impact of backwash in a single medium rapid sand filter treating anoxic
95 groundwater at a drinking water treatment plant (DWTP) in the Netherlands. We used a combination
96 of advanced geochemical and microbiological analyses, including synchrotron X-ray spectroscopy, X-
97 ray diffraction (XRD), sequential extractions, scanning electron microscopy (SEM) and 16S rRNA gene
98 amplicon sequencing to identify the chemical and microbial processes taking place in the filter before
99 and after backwash. We found evidence for a vertical stratification of microbiological processes
100 contributing to Fe and Mn removal, while alternating Fe and Mn coatings were found on the filter
101 medium throughout the filter, implying slow mixing and thereby homogenization of the chemical
102 composition of the filter medium due to backwashing.

103 **2. Materials and methods**

104 **2.1 Drinking water treatment plant**

105 The DWTP investigated in this study is located in Laren, the Netherlands (52.24029°N, 5.20258°E) and
106 is operated by Vitens N.V. The groundwater is extracted from 9 wells (8 vertical wells and 1 horizontal
107 well) from an unconfined shallow aquifer (-13 m). The groundwater is anoxic and is mixed with slightly
108 oxygenated shallow ground water in the wells, therefore raw water contains some oxygen (~60 μM).
109 The treatment process consists of three steps, including aeration, single medium rapid sand filtration
110 and granular activated carbon filtration (Supplementary Figure 1).

111 The DWTP operates two rapid sand filters in parallel, each with an area of 40 m^2 and a filter medium
112 thickness of ~2 m. The sand has an average diameter of 1.7-2.5 mm (porosity ~42%) and density of 2.6
113 g/cm^3 . The supernatant level which is controlled with a valve in the outflow of the filter, is between 30-
114 40 cm above the filter bed. The feed flow is ~220 m^3/h . One filter (Filter 1) was investigated in this
115 study and has been in operation with this sand filter material since 2014, when the sand was replaced
116 after ~25 years of operation. The DWTP is not continuously operational, with production periodically
117 being halted when drinking water demands are lower. The annual production rate for Filter 1 is ~1 000
118 000 m^3 .

119 Filters are backwashed after 16 000-18 000 m³ water has been produced (every ~72 to 82 h). This
120 cleaning procedure has a duration of 19.5 minutes and consists of the following steps: 1 minute of water
121 backwash (water velocity of 21 m/h), 12 minutes of air and water backwash (air velocity of 60 m/h,
122 water velocity of 20 m/h and) and 6.5 minutes of water backwash (water velocity of 40 m/h). The
123 backwash does not lead to overall bed expansion.

124 The pressure difference in the filter during a filter run is monitored continuously by the drinking water
125 company using piezometers in the top and bottom of the filter. The pressure difference data for two
126 backwash cycles which sampling was conducted in November 2021 were analyzed in this study. We
127 also calculated the Fe load between two backwash cycles based on raw water concentrations and the
128 total volume filtered, and assessed whether there was a relationship between the Fe load and pressure
129 buildup.

130 **2.2. Sample collection**

131 Water samples were collected in November 2021 at five different times in a backwash cycle, first at the
132 end of the runtime (74 h), then at four different time points after backwash (2 h, 25 h, 29 h and 43 h).
133 Filter medium samples were obtained just before and after backwash (74 h, 0 h). Backwash suspension
134 samples were collected every 1 min during the backwash procedure.

135 Extracted groundwater (“raw water”) was collected prior to aeration. Filter influent water was collected
136 directly from the supernatant water above the filter. To assess Fe²⁺, Mn²⁺ and NH₄⁺ removal in the filter,
137 water samples were obtained from 6 taps available at the side of Filter 1 at 50, 80, 110, 140, 170 and
138 200 (bottom of filter) cm depth. Filter effluent water was sampled from a tap exiting under the filter
139 effluent chamber.

140 The pH, O₂, conductivity and temperature were measured directly in the water from the taps with a
141 HQ40D Portable Multimeter (HACH), with a tube from each tap leading directly into a plastic bottle
142 that overflowed continuously. Unfiltered and filtered (0.45 μm) water samples were collected in 15 mL
143 centrifuge tubes and acidified with ultra-pure nitric acid (HNO₃; 10 μL per 1 mL of sample) and stored

144 at 4 °C for analysis of total and dissolved Fe and Mn. For the analysis of NH_4^+ , NO_2^- and NO_3^- , separate
145 filtered water samples were collected and stored at -20 °C.

146 A stainless-steel peat sampler (Veenlans 04.09, Royal Eijkelkamp) was used to collect sand samples at
147 the following sand filter depth intervals for analysis of the geochemistry and microbiology: 0-2 cm, 4-
148 6 cm, 10-15 cm, 15-20 cm, 25-30 cm, 30-40 cm, 40-50 cm, 50-60 cm, 60-70 cm, 70-80 cm, 80-90 cm,
149 90-100 cm, 100-110 cm, 110-120 cm, 120-130 cm, 130-140 cm, 140-150 cm, 150-160 cm and 160-170
150 cm. The sand samples were stored in 50 ml centrifuge tubes in a freezer (-20°C) until analysis.

151 **2.3. Analysis of water chemistry**

152 Total and dissolved Fe (Limit of Detection [LOD] = 0.4 μM) and Mn (LOD = 0.018 μM) were analyzed
153 using a Perkin-Elmer Avio 500 Inductively Coupled Plasma Optical Emission Spectrophotometer (ICP-
154 OES). The difference between total and dissolved Fe and Mn was used as a measure of particulate Fe
155 and Mn. The concentration of NH_4^+ (LOD = 0.3 μM), NO_2^- (LOD = 0.02 μM) and NO_3^- (LOD = 0.09
156 μM) in the filtered water samples was determined spectrophotometrically with a Gallery™ Discrete
157 Analyzer. NO_x was measured as described in Jumppanen et al. (2014), and NH_4^+ according to ISO7150-
158 1:1984.

159 **2.4. Geochemical analysis of filter medium**

160 The type of Fe and Mn-oxides present on the coatings before and after backwash was determined using
161 a three-step sequential extraction procedure with ascorbic acid, 1M HCl and CDB (Claff et al., 2010;
162 Lenstra et al., 2021; Raiswell et al., 2010). The first extraction step with ascorbic acid primarily
163 dissolves Fe from poorly crystalline Fe-oxides (e.g., ferrihydrite) and Mn-oxides (e.g., birnessite). The
164 second extraction step dissolves minerals sensitive to low pH, including carbonates and poorly ordered
165 oxides, and the third step dissolves crystalline Fe-oxides. The filter medium was freeze-dried prior to
166 extraction. Approximately 100-250 mg of filter medium and 10 ml extractant were used in each step.
167 All samples were analyzed with ICP-OES to determine Fe and Mn content.

168 For high-resolution imaging, coating thickness measurements and elemental mapping of coating
169 characteristics, a Zeiss EVO 15 environmental SEM with energy dispersive X-ray spectroscopy (EDS)

170 was used. Filter medium from 5-10 cm and 150-160 cm in the filter bed was analyzed, from samples
171 taken before (74 h) and after backwash (0 h). Selected samples were freeze-dried and fixed to 0.5-inch
172 aluminum SEM specimen stubs (Agar Scientific Ltd.) using a conductive carbon glue. Mounted
173 samples were coated with 15 nm of platinum using a 208HR Sputter Coater. Particles from backwash
174 water (taken after 7 minutes of backwashing) were processed and analyzed in a similar manner.

175 Filter medium from 15-20 cm depth in the filter was embedded in epoxy resin (2.5 cm) and polished to
176 expose cross sections of the sand grains and coatings at the surface. The sample was investigated using
177 μ -XRF and μ -X-ray absorption spectroscopy at Fe and Mn K-edges at the ID21 beamline (Salomé et
178 al., 2013) at the European Synchrotron Radiation Facility (ESRF) in Grenoble, France. The beam was
179 focused to $0.7\mu\text{m ver.} \times 0.8\mu\text{m hor.}$ using a Kirkpatrick Baez mirrors system. The samples were mounted
180 vertically, with an angle of 62° with respect to the incident beam. X-ray energy of the incoming beam
181 was selected and tuned by means of a horizontal deflecting double-mirror system (Si coating for
182 harmonics rejection) and a Si (111) monochromator ($\Delta E/E \sim 2.10^{-4}$). The beam intensity was monitored
183 continuously using a photodiode placed upstream of the sample. XANES spectra were acquired in XRF
184 mode, using a large area (80 mm^2 collimated active area) Silicon Drift Diode (Bruker, Karlsruhe,
185 Germany). At selected spots, X-ray absorption spectra in fluorescence mode were collected within the
186 corresponding energy range, 6.50– 6.90 keV and 7.00–7.65 keV for Mn and Fe, respectively. The
187 monochromator energy was calibrated based on the maximum intensity of the first derivative of Mn
188 foil at 6.53862 keV for Mn and Fe foil at 7.11198 keV for Fe. X-ray fluorescence spectra were processed
189 and I_0 normalized using the PyMca X-ray Fluorescence Toolkit (Sole´et al., 2007) to produce elemental
190 maps. Spectra for analyzing the X-ray absorption near edge structure (XANES) and extended X-ray
191 absorption fine structure (EXAFS) were normalized and extracted using the ATHENA software
192 package (version 0.8.056 Ravel and Newville, 2005).

193 Consecutively collected Mn-XANES spectra at one spot exhibited a shift of the edge to lower energies
194 and a decrease in white line intensity, indicating photoreduction of Mn-oxides (Supplementary Figure
195 2). For this reason only the first spectrum was used for further analysis, assuming that the effect of
196 photoreduction was negligible for this spectrum. Normalized Fe and Mn XANES spectra, collected at

197 different spots on the sample, varied for the respective element regarding the amplitude of oscillations,
198 shape and position of the edge, and the magnitude of the pre-edge feature. These differences could not
199 be solely ascribed to differences in speciation but are also caused by self-absorption. To correct for self-
200 absorption the XANES(Fluo) algorithm a correction method developed by Daniel Haskel implemented
201 in Athena was used (Haskel, 1999). As the exact composition at the measured spots was not known the
202 correction was made based on $\text{Fe}(\text{OH})_3 \cdot n(\text{H}_2\text{O})$ and $\text{MnO}_2 \cdot n(\text{H}_2\text{O})$, respectively. The number of water
203 molecules was adjusted until the magnitude of the pre-edge feature and the amplitude of the white line
204 was similar to those of the selected reference spectra showing strong resemblance with the spectra from
205 the sample. Differences among spectra remaining after this correction should then be indicative for
206 differences in speciation. \

207 The mineralogy of Fe and Mn-oxide coatings from selected samples from the top (2-4 cm), middle (90-
208 100 cm), and bottom (150-160 cm) of the filter was determined by XRD. Freeze dried samples were
209 ground using a mortar and pestle and sieved to obtain the fraction $< 50 \mu\text{m}$ and subsequently placed
210 onto a PMMA sample holder with a cavity diameter of 25 mm. XRD spectra were obtained with a
211 Bruker D8 Advance with a LYNXEYE detector and a θ/θ goniometer with Cu-K α radiation ($\lambda =$
212 1.54056 \AA) with the tube operated at 40 kV and 40 mA. We used a primary Soller slit of 2.5° , a
213 motorized divergence slit that illuminates 20 mm of the sample, resulting in a constant irradiated
214 surface, and a motorized anti-scatter screen. X-ray powder diffraction patterns were recorded from 3 to
215 $80^\circ 2\theta$, in 0.02° steps, and counting for 0.85 s per step. Samples were spun continuously during
216 measurement (0.25 Hz). Samples were compared to standards, including those of quartz and feldspar
217 minerals and, Fe and Mn-oxides(e.g. birnessite and ferrihydrite) for identification.

218 Specific surface areas of selected filter medium samples from 2-4 cm, 50-60 cm, 100-110 cm, and 150-
219 160 cm were measured using the Brunauer-Emmett-Teller (BET) nitrogen gas adsorption method
220 (relative pressure range 0.05–0.25) with a Quanta chrome Autosorb-6B gas adsorption analyzer at 77
221 K. Results were normalized to the density of the filter material. Before the surface area measurement,
222 the samples were exposed to a vacuum for 40 hours at 60°C .

223 **2.5. DNA isolation and 16S rRNA gene amplicon sequencing**

224 For analysis of the microbial community before and after backwash (74 h and 0 h), sand samples of the
225 filter medium were analyzed from the following depth intervals for spatial coverage: 0-2 cm, 4-6 cm,
226 10-15 cm, 25-30 cm, 40-50 cm, 70-80 cm, 80-90 cm, 110-120 cm, 130-140 cm, 160-170 cm.

227 Genomic DNA was extracted from samples of 0.5 g (wet weight) using the DNeasy Powersoil DNA
228 isolation kit (QIAGEN, Hilden, Germany). Cell lysis was performed by bead beating at 50 Hz for 1 min
229 using a TissueLyser LT (QIAGEN, Hilden, Germany). When insufficient amounts of DNA were
230 obtained, up to four replicates using 0.5 g sample material each were pooled on one GeneJet Spin
231 column. In addition to 800 μ L CD1 solution, 500 μ L of 10 % w/v skimmed milk (Sigma-Aldrich) was
232 added to the Powerbead Pro tubes. The skimmed milk solution was autoclaved for 5 min at 121 °C,
233 which proved long enough to avoid isolating DNA from the skimmed milk itself, and short enough to
234 avoid excessive caramelizing of the skimmed milk solution (Corbera-Rubio et al., 2023). Prior to DNA
235 elution in 100 μ L DEPC water, the column was incubated with DEPC water for 1 min at room
236 temperature.

237 16 rRNA gene amplicon sequencing was performed by Macrogen Inc. (Seoul, South Korea) using the
238 Illumina MiSeq platform. Primers used for bacterial 16S rRNA gene amplification were 341F (5'-
239 CCTACGGGNGGCWGCAG-3'; Herlemann et al., 2011) and 806R (5'-
240 GGACTACHVGGGTWTCTAAT-3'; Caporaso et al., 2012). Paired end libraries were constructed
241 using the Herculase II Fusion DNA Polymerase Nextera XT Index Kit V2 (Illumina, San Diego, USA)
242 with the 16S Metagenomic Sequencing Library Preparation Part # 15044223 Rev. B protocol. Between
243 100.000 and 260.000 paired end reads were obtained per sample. The data was processed in R (v3.5.1;
244 R Core Team, 2019) using the DADA2 pipeline (v1.8; Callahan et al., 2016). The 16S rRNA gene-
245 based taxonomy was obtained using the SILVA database (release 138.1, Quast et al., 2012). The relative
246 abundances as calculated using DADA2 were analyzed using the R package Phyloseq (v1.30.0;
247 McMurdie & Holmes, 2013). For data visualization in bar plots, families and genera were included that
248 constituted >1% and 1.5% relative abundance, respectively, in at least two of the samples.

249 3. RESULTS

250 Before backwash (i.e. 74 hours after the previous backwash cycle), the filter was covered with a 1-2 cm
251 thick layer of fine orange flocs (Figure 1 A). The color of the filter medium was reddish-brown in the
252 top 30 cm of the filter and gradually transitioned to blackish-brown between ~50 and 160 cm depth
253 (Figure 1 B). Directly after backwash, the orange layer of fine material on top of the filter was no longer
254 present and the color of the upper 30 cm of the filter was much browner (Figure 1C). The deeper parts
255 of the filter (below 50 cm depth) remained predominantly blackish-brown (Supplementary Figure 3).

256 3.1. Water chemistry and filter functioning

257 The supernatant of the sand filter was always well-oxygenated ($>280 \mu\text{M O}_2$; Table 1) because of the
258 aeration of abstracted anoxic groundwater prior to the sand filtration step. In the sand filter, oxygen
259 concentrations decreased with depth, but never reached values below $193 \mu\text{M}$ (Figure 2). Only minor
260 variations in pH were observed, with values ranging from 7.2 to 7.4. The conductivity of the water
261 decreased with depth in the filter (by ~ 10 units), in line with the removal of solutes. Both NH_4^+ and
262 NO_3^- were present in the raw water (~ 34 and $50 \mu\text{M}$, respectively). All NH_4^+ was converted to NO_3^- in
263 the sand filter (Table 1; Supplementary Figure 4).

264 Iron in the raw water was mostly present in dissolved form (Table 1). At the end of a filter run,
265 particulate Fe dominated in the supernatant of the sand filter. After backwash, however, Fe in the
266 supernatant of the sand filter was primarily dissolved (Figure 2). The Fe data for 25 and 43 h hours after
267 backwash show that the proportion of particulate Fe increased at the expense of dissolved Fe during the
268 filter run. Most Fe removal ($> 95\text{-}99\%$) occurred in the top 50 cm of the filter at the investigated time
269 points (Table 1 and Supplementary Data S2).

270 Manganese occurred only in dissolved form and is, therefore, assumed to be present as Mn^{2+} .
271 Manganese was removed between a depth of 0 and 110 cm depth, in parallel with NH_4^+ (Figure 2). At
272 50 cm depth in the filter, only $\sim 52\%$ of the incoming Mn was removed. The depth of Mn removal and
273 the removal efficiency did not change during the investigated time points of a filter run (Supplementary
274 Data S1).

275 With increasing runtime, an increase in pressure across the filter from 1,5 kPa to 14 kPa was observed
276 (Figure 3), which strongly correlated with the Fe load ($R^2= 0.93$; Supplementary Data S3). After
277 backwashing, the pressure across the filter was restored to 1 kPa.

278 3.2 Filter medium

279 Most Fe-oxides were extracted in the ascorbic acid step, while Mn-oxides were mostly dissolved in HCl
280 (Supplementary Table 1). The ratio of the total Mn:Fe extracted was close to 1, with an average of ~ 680
281 $\mu\text{mol/g}$ Fe and ~ 674 $\mu\text{mol/g}$ Mn-oxides present throughout the filter before and after backwash
282 (Supplementary Table 1). If we combine the Fe and Mn load for the filter (see section 2.1, assuming a
283 bulk filter material density of 2.6 g/cm^3 and 7 years of operation) with the total amount of Fe and Mn
284 measured in the filter (average before and after backwash), we find that $\sim 17\%$ of the Fe and $\sim 63\%$ of
285 the Mn that entered the filter accumulated there. This implies that $\sim 83\%$ of the Fe and $\sim 37\%$ of the Mn
286 was removed from the filter through backwash (Supplementary Table 1, Supplementary Data S4).

287 The thickness of the mineral coatings ranged from ~ 80 to ~ 200 μm . Before backwash, Fe-oxides
288 dominated the coating surface in the top 30 cm of the filter (Figure 4, top 5 cm). After the filter was
289 backwashed, a mix of both Fe and Mn-oxide surface-coated grains were found in the top of the filter.
290 The Fe-oxides consisted of globular nodules < 1 μm , while Mn-oxides appeared as sponge/coral like
291 structures of 1-13 μm in diameter (Supplementary Figure 5 and 6).

292 Cross-sections of the coatings revealed that they consisted of alternating layers of Fe and Mn-oxides
293 (Figure 4). The alternating coatings were found on filter medium grains originating from both the
294 surface (top 5 cm) and bottom samples (150 cm). Given the more than seven years of operation of the
295 sand filter at the time of sampling, this suggests slow mixing of the filter medium over the full filter
296 depth, and not only the top ~ 50 cm. The Mn-oxide layers were more porous compared to the denser
297 Fe-oxide layers (Supplementary Figure 7). The BET specific surface area of the filter medium was
298 similar across all depths of the filter ($\sim 3.4 \cdot 10^7 \text{ m}^2/\text{m}^3$; Supplementary Data S5).

299 Remnants of hollow sheets, characteristic for the iron-oxidizer *Leptothrix* (Emerson et al., 2010) and
300 twisted stalks resembling those known for *Gallionella* (Chan et al., 2010) were detected on the metal

301 coated surface of the filter medium, and, occasionally, were found to be intertwined within the filter
302 medium coating (Figure 5). The hollow sheets were far more dominant compared to the twisted stalks,
303 with the highest abundance in the top 30 cm of the filter. EDS imaging confirmed that the hollow sheets
304 mainly consist of Fe-oxides (Figure 5B). Bacterial filaments on the filter medium coating, recognizable
305 by their enrichment in carbon, were also detected (Figure 5A).

306 Self-absorption corrected XANES and EXAFS spectra of Fe and Mn collected along a transect through
307 the coating did not show significant differences (Figure 6). This indicates that the redox state and
308 speciation of Fe and Mn in the coating is very similar, irrespective of position and, hence, age and
309 change in composition. Upon comparison with spectra from a variety of Fe-oxides the XANES spectra
310 and the part of the EXAFS spectra with acceptable quality ($k < 7 \text{ \AA}^{-1}$) showed closest resemblance with
311 the spectrum FhSi*. This spectrum is a combination of spectra collected from Fe(III) precipitates
312 formed upon the oxidation of Fe^{2+} in the presence of 0.5 mM silicic acid in Na and Ca containing
313 background electrolyte (Senn et al., 2015). These precipitates are generally poorly ordered and
314 characterized by a lower degree of corner-sharing polymerization compared to 2L ferrihydrite,
315 synthesized in the absence of Si. The position of edge of the Mn XANES spectra indicates that Mn is
316 predominately in the form of Mn(IV) and the XANES and EXAFS spectra showed closest resemblance
317 with those of hexagonal birnessite produced by Mn(II) oxidation by *Pseudomonas putida*. However,
318 the quality of the EXAFS spectrum beyond $k \ 8 \text{ \AA}^{-1}$ was insufficient to unequivocally identify the
319 structure of the phylломanganates as distinctive features in the EXAFS spectra are located in that region
320 (Webb et al. 2005).

321 No sharp peaks other than those attributed to quartz and feldspar (microcline) could be identified in the
322 X-ray diffractograms (Supplementary Figure 8). This is in line with the findings from XAS analysis as
323 ferrihydrite-like precipitates and biogenic birnessite only produce broad peaks with low amplitude
324 (Cornell & Schwertmann, 2003; Villalobos et al., 2003)

325 SEM analysis of the backwash suspension showed that the backwash process mainly removed Fe-flocs
326 and we observe bacterial Fe-deposit structures mainly in the form of hollow sheets. Furthermore, some

327 Mn-oxides were detected in these Fe-flocs, indicating that Mn was also removed during backwash
328 (Supplementary Figure 8).

329 3.3 Microbiology

330 The results of 16S rRNA gene amplicon sequencing revealed distinct variations in the microbial
331 community with filter depth that largely remained undistributed by the backwashing procedure (Figure
332 7). Before backwash, *Gallionella* was the most abundant genus in the upper 30 cm of the filter (40%
333 and 20% at 2 cm and 30 cm, respectively), but decreased in relative abundance with depth to 0.4% at
334 the bottom of the filter. Below 40 cm, *Candidatus Nitrotoga* constituted the most abundant genus in the
335 *Gallionellaceae* family (Supplementary Figure 10). Additionally, the genera *Leptothrix* and
336 *Sideroxydans* were present at 3-6% and 3-7%, respectively, with the highest abundance in the top 30
337 cm.

338 The relative abundance of *Nitrospira* increased with depth in the filter, accounting for ~5% across the
339 top 30 cm to ~18% at 160 cm depth. Generally, the microbial community below 100 cm depth was more
340 diverse than in the top of the filter (Figure 7).

341 Just after the filter was backwashed, the abundance of *Gallionella* in the top of the filter decreased (from
342 45% to 20% at cm depth), while the relative abundances of *Sideroxydans* and *Leptothrix* did not
343 decrease. The relative abundance of *Nitrospira* increased in the first 30 cm of the filter, from ~5% to
344 ~7% before and after backwash, respectively. Generally, the microbial community below 25-30 cm
345 depth in the filter remained unchanged after backwash, as supported by nonmetric multidimensional
346 scaling (NMDS) analysis, which showed samples from similar depths from before and after backwash
347 clustering together (Supplementary Figure 11).

348 4. DISCUSSION

349 4.1 Mechanisms of Fe and Mn removal

350 In this study, we show that both Fe^{2+} and Mn^{2+} are successfully removed during drinking water
351 production from abstracted groundwater, using one single-media rapid sand filtration step. This removal
352 is the result of a combination of both chemical and microbiological processes and requires regular
353 backwashing to counteract pressure buildup in the filter.

354 Because of fast oxidation of Fe^{2+} under oxygenated conditions (Gude et al., 2018), most Fe^{2+} is removed
355 in the supernatant and settles as Fe-flocs and microbially formed Fe-oxides on the filter bed (Figure 1,
356 Figure 5). As the water flows through the filter bed, globular nodules of Fe-oxides are formed on the
357 filter medium in the form of coatings, indicating that heterogeneous Fe^{2+} oxidation also plays an role in
358 Fe^{2+} removal (Supplementary Figure 5).

359 *Gallionella*, *Leptothrix* and *Sideroxydans* are genera known to harbor iron-oxidizing species that
360 oxidize Fe^{2+} and dominate the top 30 cm of the filter (Figure 7). This dominance, together with the
361 observation of hollow sheets and twisted stalks indicative of biological iron-oxidation implies that
362 microorganisms contribute to Fe^{2+} removal at this DWTP (Figure 5). Even though some *Leptothrix*
363 species can oxidize both Fe^{2+} and Mn^{2+} (Fleming et al., 2014; Zhang et al., 2002), our SEM-EDS
364 mapping only reveals Fe-rich bacteriological hollow sheets, suggesting that *Leptothrix* mainly convert
365 Fe^{2+} in the studied filter (Figure 5). Some iron-oxidizing bacteria may enter the filter through the
366 groundwater, as the raw water is mixed with oxygenated water in the wells already. Despite the general
367 perception of Fe(II) oxidation being microaerophilic (e.g. Maisch et al., 2019), their presence and
368 activity at higher O_2 concentrations, as observed here ($[\text{O}_2] = >70 \mu\text{M}$; Table 1; Figure 2), is common
369 in drinking water treatment plants (de Vet et al., 2011; Gülay et al., 2018; Sharma et al., 2005; Van
370 Beek et al., 2016). Raw water containing iron-oxidizing bacteria has previously also been observed at
371 other treatment locations (Pacini et al., 2005). The temperature of $\sim 11^\circ\text{C}$ in the DWTP may further
372 stimulate microbial iron-oxidation as suggested in other studies (de Vet et al., 2011; Gülay et al., 2018).
373 Notably, the bacterial production of Fe-oxides in the form of stalks and sheets may allow for longer

374 runtimes, as bacterially produced Fe-oxides is slightly less voluminous compared to Fe-flocs formed
375 through chemical precipitation (Sharma et al., 2005).

376 Both the solute and solid phase analyses indicate that removal of Mn^{2+} occurs down to a depth of 110
377 cm, in parallel with NH_4^+ removal (Figure 2). The groundwater at this DWTP contains $\sim 20 \mu M Mn^{2+}$,
378 which is a relatively high concentration compared to those elsewhere (Tekerekopoulou et al., 2013).
379 We note that the presence of NH_4^+ ($\sim 30 \mu M$) does not negatively affect Mn^{2+} removal. This is in
380 agreement with other studies showing that when NH_4^+ concentrations are below $\sim 40 \mu M$, Mn^{2+} and
381 NH_4^+ can be removed in parallel (Tian et al., 2019). However, at higher NH_4^+ concentrations, Fe^{2+} and
382 NH_4^+ removal typically occurs before Mn^{2+} removal (Corbera-Rubio et al., 2023). While the effect of
383 high NH_4^+ concentrations on Mn^{2+} removal was previously linked to variations in O_2 and pH associated
384 with nitrification (Gouzinis et al., 1998; Tian et al., 2019), other chemical, physical and/or
385 microbiological factors likely also play a role in achieving successful Mn^{2+} removal in the presence of
386 NH_4^+ (Haukelidsaeter et al., 2023).

387 Microbial Mn^{2+} oxidation is crucial in facilitating the removal of Mn^{2+} in the studied filter, as indicated
388 by the dominance of Mn(IV) containing phyllophanes in the oxide coatings (Figure 6). Although
389 we cannot exclude that heterogeneous oxidation of Mn occurs in the filter, the characteristic of Mn(III)
390 and Mn(II)/Mn(III)-oxides with distinctively different XANES and EXAFS spectra were not found
391 (Figure 6; Inoué et al., 2019; Murray et al., 1985). This contrasts with previous work on other DWTPs,
392 which suggested heterogeneous oxidation of Mn^{2+} dominates after a mineral coating is established on
393 the filter medium (Bruins et al., 2015). Members of the genus *Hyphomicrobium* are commonly
394 encountered at drinking water facilities where Mn^{2+} is removed (Albers et al., 2015; Haukelidsaeter et
395 al., 2023). While they may be involved in Mn^{2+} oxidation at this site, their abundance was low in the
396 filter (Figure 7). Additionally, the possibility for Mn^{2+} oxidation by nitrifying bacteria has been raised
397 (Vandenabeele et al., 1995), which could match the simultaneous removal of Mn^{2+} and NH_4^+ as
398 observed here (Figure 2) and the large relative abundance of especially the genus *Nitrospira* (Figure 7).
399 However, based on 16S rRNA gene amplicon sequencing alone, we cannot deduce the microorganisms
400 responsible for Mn^{2+} oxidation in this rapid sand filter.

401 The microbial depth stratification observed in the filter cannot be explained purely by thermodynamics,
402 but rather indicates that there are unknown microbial and chemical interactions determining the
403 sequence of microbial Fe^{2+} , Mn^{2+} and NH_4^+ oxidation in the rapid sand filters (Figure 2; Figure 7). In
404 the top of the filter, iron-oxidizing bacteria need to rapidly oxidize Fe^{2+} in order to compete with
405 chemical oxidation of Fe^{2+} (Emerson et al., 2010). Notably, Fe^{2+} oxidation precedes NH_4^+ oxidation in
406 the filter, even though the latter process is thermodynamically more favorable (-58 kJ/mol for Fe^{2+} vs
407 -349 kJ/mol for complete NH_4^+ oxidation; Emerson et al., 2010; Van Kessel et al., 2015). The inhibition
408 of NH_4^+ removal by Fe has previously been observed in other drinking water filters (de Vet et al., 2009).
409 The exact nature of this interaction has not yet been identified, however.

410 Subsequent removal of NH_4^+ , occurring either prior to or at the same time as Mn^{2+} removal has also
411 been observed at other DWTPs (Corbera-Rubio et al., 2023; Gouzinis et al., 1998; Tian et al., 2019).
412 Again thermodynamics cannot fully explain this (-68 kJ/mol for oxidation of Mn^{2+} vs -349 kJ/mol for
413 complete NH_4^+ oxidation; Yu & Leadbetter, 2020 ; Van Kessel et al., 2015), hence we assume that also
414 here other, yet unidentified factors regulate this sequence. As the common terminal electron acceptor
415 in all these reactions is O_2 , and O_2 never becomes limiting in the investigated filter, its availability
416 cannot be a cause of the zonation of microbial processes.

417 Importantly, the vertical structure of the microbial community within the rapid sand filter in this study
418 exhibits a greater variation over depth compared to that of two other DWTPs (Figure 6; Corbera-Rubio
419 et al., 2023). This difference may be attributed to variations in backwash regimes implemented at these
420 other locations and/or lower spatial sampling resolution with depth. Overall, the microbial depth
421 distribution achieved here shows that regularly backwashed rapid sand filters can be biologically more
422 heterogeneous than previously assumed.

423 **4.2 Effect of backwash**

424 The removal efficiency of the sand filter for Fe^{2+} and Mn^{2+} did not change during a filter run (Figure
425 2). Hence, the backwash primarily restored efficient flow in the filter (Figure 3). Without backwash,

426 the pressure buildup in the filter would probably result in irregular and preferential flow through the
427 bed and uncontrollable supernatant level, which would negatively affect both Fe and Mn removal.

428 Despite higher concentrations of Fe in the raw water when compared to Mn (Table 1; Figure 2), we
429 show that the metal oxide coatings were equally enriched in Fe and Mn (Supplementary Table 1). The
430 more efficient removal of Fe is the result of a difference in the removal mechanisms of Fe and Mn:
431 while both Fe and Mn form coatings on the filter medium, Fe additionally forms flocs in the supernatant
432 Both the flocs and Fe and Mn-coatings are removed during backwash, together with mainly hollow
433 sheets formed by iron-oxidizing bacteria (Supplementary Figure 9).

434 We show that one backwashing event leads to substantial mixing of the upper 30 cm of the filter
435 medium, while keeping both the stratification of the microbial community (Figure 7) and the color
436 gradient below a depth of 30 cm in the filter largely intact (Figure 1). The most prominent change in
437 the microbial community was the decrease in relative abundance of *Gallionella* in the top of the filter
438 after backwash, indicating preferential loss of these iron-oxidizing bacteria.

439 The presence of layered Fe and Mn-oxide coatings, along with relatively uniform coatings throughout
440 the height of the filter bed, indicates that slow mixing processes occur over time scales far beyond a
441 single backwash cycle (Figure 4, Supplementary Table 1). This is consistent with other studies
442 indicating random grain displacement, eventually resulting in a more even distribution of the grains
443 (Ramsay et al., 2021), and a homogenous chemical composition of the filter (Corbera-Rubio et al.,
444 2023; Sharma et al., 2002). However, the clear stratification of the microbial community, indicates that
445 full mixing is slower than bacterial regrowth within the different depths of the filter (Figure 7).

446 The resulting uniform growth of the filter bed, stimulated by multiple backwash cycles is likely
447 important for the hydrological performance of the filter (Ramsay et al., 2021). A well-sorted medium
448 ensures a more homogeneous flow through the filter and increases the contact time between water and
449 sand grains, which is especially crucial for effective Mn^{2+} removal (Haukelidsaeter et al., 2023).

450 **4.3 Coating growth and ageing of rapid sand filters**

451 Based on the measured coating thicknesses, a coating growth rate of 9-28 $\mu\text{m}/\text{year}$ of the filter medium
452 can be estimated (Figure 6). A thick coating has been proven to be beneficial for microorganisms, such
453 as nitrifiers, that colonize the outer periphery of the coating which acts as a protective layer during
454 backwash (Gülay et al., 2014). We find that Mn-oxides are more porous than Fe-oxides, hence Mn-
455 oxide coatings might provide more attachment surfaces for microorganisms. Because ~50% of the
456 coating in the filter studied here consists of Mn-oxides, it is expected that at DWTPs where Mn^{2+}
457 concentrations are lower and where the filter is operated under similar conditions, coatings on filter
458 medium would have a lower rate of formation.

459 Combined X-ray characterization show that the Fe-oxide coating mainly consisted of ferrihydrite-like
460 precipitates, which is in line with other research (Sharma et al., 2002). Ferrihydrite is
461 thermodynamically more unstable compared to more crystalline oxyhydroxides, however the combined
462 effect of the presence of Si and Ca during Fe^{2+} oxidation and precipitation can effectively retard aging
463 of the precipitates and the formation of more stable phases (Senn et al., 2015), and likely also contribute
464 to the preservation of the initially formed precipitates in the sand filter.

465 With time, the thickness of the filter medium coating increases. Once the grain sizes exceed a diameter
466 of 3 mm (nearly 50% growth) the expansion of the bed during backwash can become inefficient,
467 necessitating filter replacement.

468 **4. CONCLUSIONS AND IMPLICATIONS FOR DRINKING WATER**

469 **PRODUCTION**

470 We find that chemical and biological removal mechanisms contribute to Fe and Mn at the drinking
471 water treatment plant (DWTP) studied here. We show that biological removal processes play a role in
472 Fe^{2+} removal, with iron-oxidizers such as Gallionella, Leptothrix, and Sideroxydans contributing to Fe
473 removal, mainly in the upper 30 cm the filter. The uniformity of the birnessite(IV) minerals suggest
474 microbial Mn^{2+} oxidation.

475 Our research highlights that the effectiveness of Fe and Mn removal from anoxic groundwater in
476 drinking water production using single-media rapid sand filters strongly depends on the following
477 factors:

- 478 1. **Raw water characteristics:** The initial concentrations of Fe and Mn can significantly impact
479 the filtration efficiency and rate of coating formation, as Mn contributes more to coating
480 formation compared to Fe. We observe that, at least at low NH_4^+ concentrations, Mn and NH_4^+
481 were removed in parallel.
- 482 2. **Regular backwashing:** Implementing an appropriate backwash procedure is vital for
483 successful Fe and Mn removal. We show that pressure increases in the filters over a runtime,
484 mainly due to the build-up of Fe-flocs that settle at the top of the filter. Backwash removes the
485 Fe-flocs and Mn-oxides, thereby sustaining water flow. In the investigated filter, a single
486 backwash cycle mainly mixed the upper ~30 cm of the filter. However, with time, backwashing
487 does slowly mix the whole filter bed ensuring homogeneous growth of the coatings in the filter
488 bed.
- 489 3. **Coating growth and coating formation:** The formation of mineral coatings improve both Fe^{2+}
490 and Mn^{2+} removal, by providing sites for heterogeneous oxidation and attachment sites for
491 microbes. The estimated rate of growth of the coating at the studied DWTP was ~9-28 μm per
492 year.

493 Based on the above, we recommend that water treatment facilities control the backwash process to
494 remove flocs without complete mixing of the filter media. This will likely be beneficial for the microbial
495 processes taking place in the filter and ensure the reliable and effective removal of Fe and Mn, and
496 ultimately provide high-quality drinking water to consumers.

497 **Acknowledgements**

498 We are grateful to Vitens N.V. for their support and collaboration during the visits to the
499 drinking water plant. We also thank J. Visser, E. Hellebrand, J.J. Mulder and A. van Leeuwen-Tolboom
500 for analytical support. This research was funded by the Netherlands Organisation for Scientific

501 Research (NWO) partnership program Dunea–Vitens: Sand Filtration (grant 17841). MAHJvK and SL
 502 were funded by NWO (016.Veni.192.062 and 016.Vidi.189.050, respectively), CPS by the European
 503 Research Council (ERC Synergy Grant 694407 MARIX).

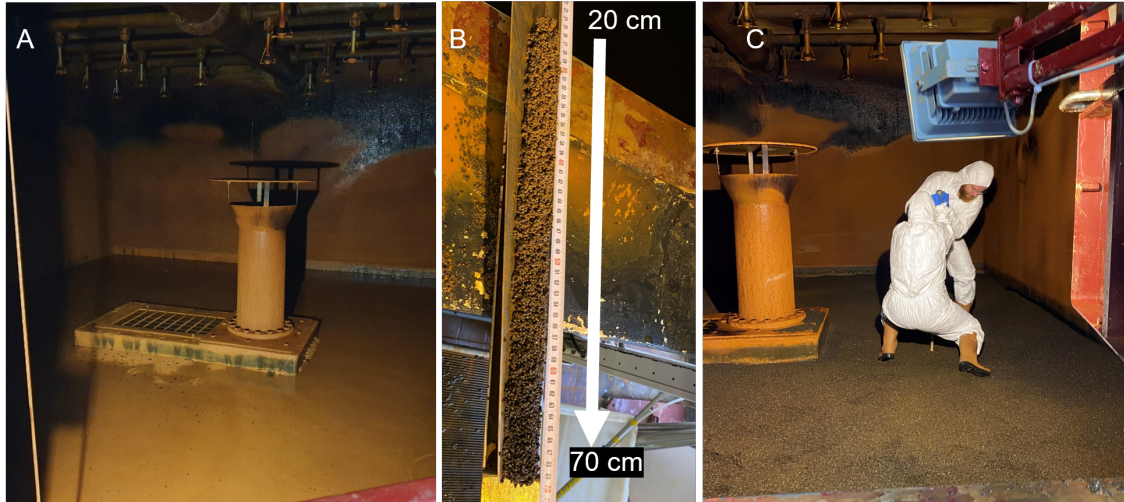
504 Reference list

- 505 Albers, C. N., Ellegaard-Jensen, L., Harder, C. B., Rosendahl, S., Knudsen, B. E., Ekelund, F., &
 506 Aamand, J. (2015). Groundwater chemistry determines the prokaryotic community structure of
 507 waterworks sand filters. *Environmental Science and Technology*, *49*(2), 839–846.
 508 <https://doi.org/10.1021/es5046452>
- 509 Bruins, J. H., Petrusovski, B., Slokar, Y. M., Huysman, K., Joris, K., Kruithof, J. C., & Kennedy, M. D.
 510 (2015). Biological and physico-chemical formation of Birnessite during the ripening of
 511 manganese removal filters. *Water Research*, *69*(0), 154–161.
 512 <https://doi.org/10.1016/j.watres.2014.11.019>
- 513 Buamah, R., Petrusovski, B., de Ridder, D., van de Wetering, T. S. C. M., & Shippers, J. C. (2009).
 514 Manganese removal in groundwater treatment: Practice, problems and probable solutions. *Water*
 515 *Science and Technology: Water Supply*, *9*(1), 89–98. <https://doi.org/10.2166/ws.2009.009>
- 516 Carta, D., Casula, M. F., Corrias, A., Falqui, A., Navarra, G., & Pinna, G. (2009). Structural and
 517 magnetic characterization of synthetic ferrihydrite nanoparticles. *Materials Chemistry and*
 518 *Physics*, *113*(1), 349–355. <https://doi.org/10.1016/j.matchemphys.2008.07.122>
- 519 Chan, C. S., Fakra, S. C., Emerson, D., Fleming, E. J., & Edwards, K. J. (2010). Lithotrophic iron-
 520 oxidizing bacteria produce organic stalks to control mineral growth: implications for biosignature
 521 formation. *The ISME Journal*, *5*(4), 717–727. <https://doi.org/10.1038/ismej.2010.173>
- 522 Claff, S. R., Sullivan, L. A., Burton, E. D., & Bush, R. T. (2010). A sequential extraction procedure for
 523 acid sulfate soils: Partitioning of iron. *Geoderma*, *155*(3–4), 224–230.
 524 <https://doi.org/10.1016/J.GEODERMA.2009.12.002>
- 525 Corbera-Rubio, F., Laurenzi, M., Koudijs, N., Müller, S., Alen, T. Van, Schoonenberg, F., Lücker, S.,
 526 Pabst, M., Loosdrecht, M. C. M. Van, & Halem, D. Van. (2023). Meta-omics profiling of full-
 527 scale groundwater rapid sand filters explains stratification of iron, ammonium and manganese
 528 removals. *Water Research*, *233*(2023), 119805. <https://doi.org/10.1016/j.watres.2023.119805>
- 529 Cornell, R. M., & Schwertmann, U. (2003). The iron oxides: Structure, properties, reactions, occurrence
 530 and uses. *Corrosion Science*, *664*. [https://doi.org/10.1016/s0010-938x\(97\)00096-6](https://doi.org/10.1016/s0010-938x(97)00096-6)
- 531 de Vet, W. W. J. M., Dinkla, I. J. T., Rietveld, L. C., & van Loosdrecht, M. C. M. (2011). Biological
 532 iron oxidation by Gallionella spp. in drinking water production under fully aerated conditions.
 533 *Water Research*, *45*(17), 5389–5398. <https://doi.org/10.1016/j.watres.2011.07.028>
- 534 de Vet, W. W. J. M., Rietveld, L. C., & Van Loosdrecht, M. C. M. (2009). Influence of iron on
 535 nitrification in full-scale drinking water trickling filters. *Journal of Water Supply: Research and*
 536 *Technology - AQUA*, *58*(4), 247–256. <https://doi.org/10.2166/aqua.2009.115>
- 537 Emerson, D., Fleming, E. J., & Mcbeth, J. M. (2010). Iron-oxidizing bacteria: an environmental and
 538 genomic perspective. *Annual Review of Microbiology*, *64*(May), 561–583.
 539 <https://doi.org/10.1146/annurev.micro.112408.134208>
- 540 Fleming, E. J., Cetinić, I., Chan, C. S., Whitney King, D., & Emerson, D. (2014). Ecological succession
 541 among iron-oxidizing bacteria. *The ISME Journal*, *8*(4), 804–815.

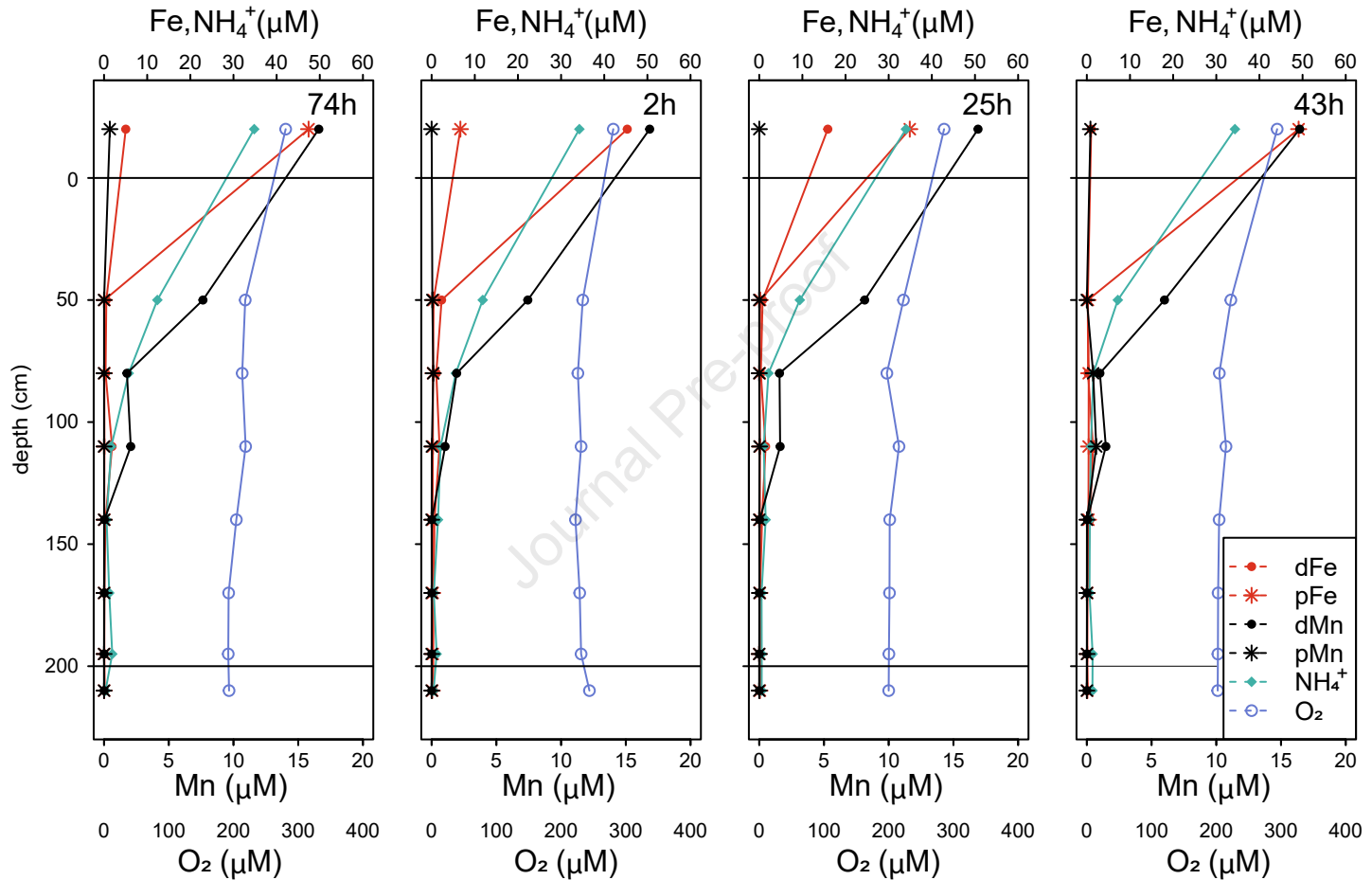
- 542 <https://doi.org/10.1038/ismej.2013.197>
- 543 Gouzinis, A., Kosmidis, N., Vayenas, D. V., & Lyberatos, G. (1998). Removal of Mn and simultaneous
544 removal of NH₃, Fe and Mn from potable water using a trickling filter. *Water Research*, 32(8),
545 2442–2450. [https://doi.org/10.1016/S0043-1354\(97\)00471-5](https://doi.org/10.1016/S0043-1354(97)00471-5)
- 546 Gude, J. C. J., Joris, K., Huysman, K., Rietveld, L. C., & van Halem, D. (2018). Effect of supernatant
547 water level on As removal in biological rapid sand filters. *Water Research X*, 1, 1–10.
548 <https://doi.org/10.1016/j.wroa.2018.100013>
- 549 Gülay, A., Çekiç, Y., Musovic, S., Albrechtsen, H.-J., & Smets, B. F. (2018). Diversity of Iron Oxidizers
550 in Groundwater-Fed Rapid Sand Filters: Evidence of Fe(II)-Dependent Growth by *Curvibacter*
551 and *Undibacterium* spp. *Frontiers in Microbiology*, 9(December), 1–14.
552 <https://doi.org/10.3389/fmicb.2018.02808>
- 553 Gülay, A., Musovic, S., Albrechtsen, H.-J., & Smets, B. F. (2013). Neutrophilic iron-oxidizing bacteria:
554 Occurrence and relevance in biological drinking water treatment. *Water Science and Technology:*
555 *Water Supply*, 13(5), 1295–1301. <https://doi.org/10.2166/ws.2013.113>
- 556 Gülay, A., Tatari, K., Musovic, S., Mateiu, R. V., Albrechtsen, H. J., & Smets, B. F. (2014). Internal
557 porosity of mineral coating supports microbial activity in rapid sand filters for groundwater
558 treatment. *Applied and Environmental Microbiology*, 80(22), 7010–7020.
559 <https://doi.org/10.1128/AEM.01959-14>
- 560 Haskel, D. (1999). *FLUO: Correcting XANES for self-adsorption in fluorescence measurements*. 1, 1–
561 14.
- 562 Haukelidsaeter, S., Boersma, A. S., Kirwan, L., Corbetta, A., Gorres, I. D., Lenstra, W. K.,
563 Schoonenberg, F. K., Borger, K., Vos, L., Wielen, P. W. J. J. Van Der, Kessel, M. A. H. J. Van,
564 Lücker, S., & Slomp, C. P. (2023). Influence of filter age on Fe, Mn and NH₄⁺ removal in dual
565 media rapid sand filters used for drinking water production. *Water Research*, 242(June), 120184.
566 <https://doi.org/10.1016/j.watres.2023.120184>
- 567 Inoué, S., Yasuhara, A., Ai, H., Hochella, M. F., & Murayama, M. (2019). Mn(II) oxidation catalyzed
568 by nanohematite surfaces and manganite/hausmannite core-shell nanowire formation by self-
569 catalytic reaction. *Geochimica et Cosmochimica Acta*, 258, 79–96.
570 <https://doi.org/10.1016/j.gca.2019.05.011>
- 571 Jumppanen, T., Jokinen, M., Airo, J., Klemm, M., Høger, D., & Suoniemi-Kähärä, A. (2014).
572 Automated Total Oxidized Nitrogen Method Using Vanadium as Reductant with Correlation to
573 Cadmium and Hydrazine Reductant Methods in Sea, Natural, and Waste Waters. *Thermo Fisher*
574 *Scientific*.
- 575 Kim, H. S., Pastén, P. A., Gaillard, J. F., & Stair, P. C. (2003). Nanocrystalline Todorokite-Like
576 Manganese Oxide Produced by Bacterial Catalysis. *Journal of the American Chemical Society*,
577 125(47), 14284–14285. <https://doi.org/10.1021/ja0375784>
- 578 Krepski, S. T., Hanson, T. E., & Chan, C. S. (2012). Isolation and characterization of a novel biomineral
579 stalk-forming iron-oxidizing bacterium from a circumneutral groundwater seep. *Environmental*
580 *Microbiology*, 14(7), 1671–1680. <https://doi.org/10.1111/j.1462-2920.2011.02652.x>
- 581 Lan, S., Wang, X., Xiang, Q., Yin, H., Tan, W., Qiu, G., Liu, F., Zhang, J., & Feng, X. (2017).
582 Mechanisms of Mn(II) catalytic oxidation on ferrihydrite surfaces and the formation of manganese
583 (oxyhydr)oxides. *Geochimica et Cosmochimica Acta*, 211, 79–96.
584 <https://doi.org/10.1016/j.gca.2017.04.044>
- 585 Lenstra, W. K., Klomp, R., Molema, F., Behrends, T., & Slomp, C. P. (2021). A sequential extraction

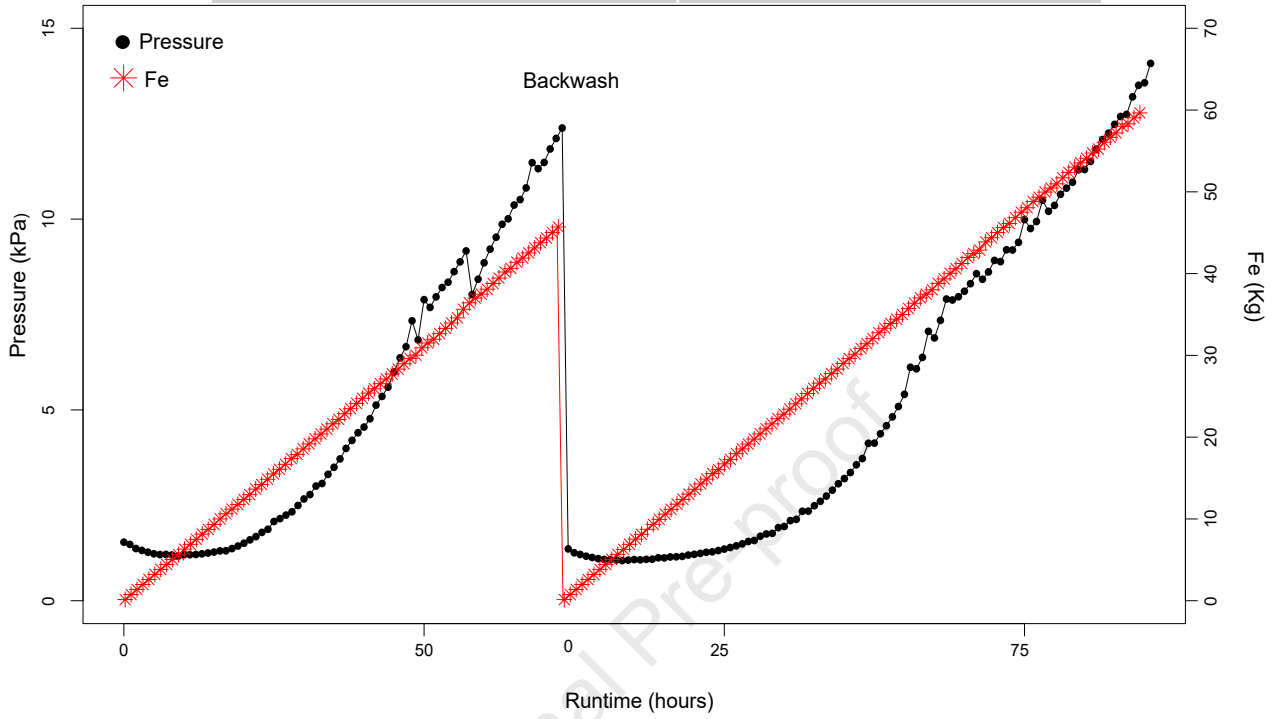
- 586 procedure for particulate manganese and its application to coastal marine sediments. *Chemical*
587 *Geology*, 584(September), 120538. <https://doi.org/10.1016/j.chemgeo.2021.120538>
- 588 Lin, C., Larsen, E. I., Nothdurft, L. D., & Smith, J. J. (2012). Neutrophilic, Microaerophilic Fe(II)-
589 Oxidizing Bacteria are Ubiquitous in Aquatic Habitats of a Subtropical Australian Coastal
590 Catchment (Ubiquitous FeOB in Catchment Aquatic Habitats). *Geomicrobiology Journal*, 29(1),
591 76–87. <https://doi.org/10.1080/01490451.2010.523446>
- 592 Maisch, M., Lueder, U., Laufer, K., Scholze, C., Kappler, A., & Schmidt, C. (2019). Contribution of
593 Microaerophilic Iron(II)-Oxidizers to Iron(III) Mineral Formation [Research-article].
594 *Environmental Science and Technology*, 53(14), 8197–8204.
595 <https://doi.org/10.1021/acs.est.9b01531>
- 596 Michel, F. M., Barrón, V., Torrent, J., Morales, M. P., Serna, C. J., Boily, J. F., Liu, Q., Ambrosini, A.,
597 Cismasu, A. C., & Brown, G. E. (2010). Ordered ferrimagnetic form of ferrihydrite reveals links
598 among structure, composition, and magnetism. *Proceedings of the National Academy of Sciences*
599 *of the United States of America*, 107(7), 2787–2792. <https://doi.org/10.1073/pnas.0910170107>
- 600 Murray, J. W., Dillard, J. G., Giovanoli, R., Moers, H., & Stumm, W. (1985). Oxidation of Mn(II):
601 Initial mineralogy, oxidation state and ageing. *Geochimica et Cosmochimica Acta*, 49(2), 463–
602 470. [https://doi.org/10.1016/0016-7037\(85\)90038-9](https://doi.org/10.1016/0016-7037(85)90038-9)
- 603 Pacini, V. A., Ingallinella, A. M., & Sanguinetti, G. (2005). Removal of iron and manganese using
604 biological roughing up flow filtration technology. *Water Research*, 39(18), 4463–4475.
605 <https://doi.org/10.1016/j.watres.2005.08.027>
- 606 Raiswell, R., Vu, H. P., Brinza, L., & Benning, L. G. (2010). The determination of labile Fe in
607 ferrihydrite by ascorbic acid extraction: Methodology, dissolution kinetics and loss of solubility
608 with age and de-watering. *Chemical Geology*, 278(1–2), 70–79.
609 <https://doi.org/10.1016/j.chemgeo.2010.09.002>
- 610 Ramsay, L., Du, F., Lund, M., He, H., & Søbørg, D. A. (2021). Grain displacement during backwash
611 of drinking water filters. *Water Science and Technology: Water Supply*, 21(1), 356–367.
612 <https://doi.org/10.2166/ws.2020.300>
- 613 Salomé, M., Cotte, M., Baker, R., Barrett, R., Benseny-Cases, N., Berruyer, G., Bugnazet, D., Castillo-
614 Michel, H., Cornu, C., Fayard, B., Gagliardini, E., Hino, R., Morse, J., Papillon, E., Pouyet, E.,
615 Rivard, C., Solé, V. A., Susini, J., & Veronesi, G. (2013). The ID21 scanning X-ray microscope
616 at ESRF. *Journal of Physics: Conference Series*, 425(PART 18), 1–5.
617 <https://doi.org/10.1088/1742-6596/425/18/182004>
- 618 Senn, A. C., Kaegi, R., Hug, S. J., Hering, J. G., Mangold, S., & Voegelin, A. (2015). Composition and
619 structure of Fe(III)-precipitates formed by Fe(II) oxidation in water at near-neutral pH:
620 Interdependent effects of phosphate, silicate and Ca. *Geochimica et Cosmochimica Acta*, 162,
621 220–246. <https://doi.org/10.1016/j.gca.2015.04.032>
- 622 Sharma, S. K., Petrushevski, B., & Schippers, J. C. (2005). Biological iron removal from groundwater:
623 A review. *Journal of Water Supply: Research and Technology - AQUA*, 54(4), 239–247.
624 <https://doi.org/10.2166/aqua.2005.0022>
- 625 Sharma, S., Petrushevski, B., & Schippers, J. C. (2002). Characterisation of coated sand from iron
626 removal plants. *Water Science and Technology: Water Supply*, 2(2), 247–257.
627 <https://doi.org/10.2166/ws.2002.0070>
- 628 Tamura, H., Kawamura, S., & Hagayama, M. (1980). Acceleration of the oxidation of Fe²⁺ ions by
629 Fe(III)-oxyhydroxides. *Corrosion Science*, 20(8–9), 963–971. [https://doi.org/10.1016/0010-938X\(80\)90077-3](https://doi.org/10.1016/0010-938X(80)90077-3)

- 631 Tebo, B. M., Bargar, J. R., Clement, B. G., Dick, G. J., Murray, K. J., Parker, D., Verity, R., & Webb,
632 S. M. (2004). Biogenic manganese oxides: Properties and mechanisms of formation. *Annual*
633 *Review of Earth and Planetary Sciences*, 32(Goldberg 1954), 287–328.
634 <https://doi.org/10.1146/annurev.earth.32.101802.120213>
- 635 Tekerlekopoulou, A. G., Pavlou, S., & Vayenas, D. V. (2013). Removal of ammonium, iron and
636 manganese from potable water in biofiltration units: A review. *Journal of Chemical Technology*
637 *and Biotechnology*, 88(5), 751–773. <https://doi.org/10.1002/jctb.4031>
- 638 Tian, X., Zhang, R., Huang, T., & Wen, G. (2019). The simultaneous removal of ammonium and
639 manganese from surface water by MeOx: Side effect of ammonium presence on manganese
640 removal. *Journal of Environmental Sciences (China)*, 77, 346–353.
641 <https://doi.org/10.1016/j.jes.2018.09.006>
- 642 Van Beek, C. G. E. M., Dusseldorp, J., Joris, K., Huysman, K., Leijssen, H., Schoonenberg Kegel, F.,
643 De Vet, W. W. J. M., Van De Wetering, S., & Hofs, B. (2016). Contributions of homogeneous,
644 heterogeneous and biological iron(II) oxidation in aeration and rapid sand filtration (RSF) in field
645 sites. *Journal of Water Supply: Research and Technology - AQUA*, 65(3), 195–207.
646 <https://doi.org/10.2166/aqua.2015.059>
- 647 Van Kessel, M. A. H. J., Speth, D. R., Albertsen, M., Nielsen, P. H., Op Den Camp, H. J. M., Kartal,
648 B., Jetten, M. S. M., & Lückner, S. (2015). Complete nitrification by a single microorganism.
649 *Nature*, 528(7583), 555–559. <https://doi.org/10.1038/nature16459>
- 650 Vandenaabeele, J., Vande Woestyne, M., Houwen, F., Germonpré, R., Vandesande, D., & Verstraete,
651 W. (1995). Role of autotrophic nitrifiers in biological manganese removal from groundwater
652 containing manganese and ammonium. *Microbial Ecology*, 29(1), 83–98.
653 <https://doi.org/10.1007/BF00217425>
- 654 Villalobos, M., Toner, B., Bargar, J., & Sposito, G. (2003). Characterization of the manganese oxide
655 produced by *Pseudomonas putida* strain MnB1. *Geochimica et Cosmochimica Acta*, 67(14), 2649–
656 2662. [https://doi.org/10.1016/S0016-7037\(03\)00217-5](https://doi.org/10.1016/S0016-7037(03)00217-5)
- 657 Vries, D., Bertelkamp, C., Schoonenberg Kegel, F., Hofs, B., Dusseldorp, J., Bruins, J. H., de Vet, W.,
658 & van den Akker, B. (2017). Iron and manganese removal: Recent advances in modelling
659 treatment efficiency by rapid sand filtration. *Water Research*, 109, 35–45.
660 <https://doi.org/10.1016/j.watres.2016.11.032>
- 661 Webb, S. M., Tebo, B. M., & Bargar, J. R. (2005). Structural characterization of biogenic Mn oxides
662 produced in seawater by the marine bacillus sp. strain SG-1. *American Mineralogist*, 90(8–9),
663 1342–1357. <https://doi.org/10.2138/am.2005.1669>
- 664 Yu, H., & Leadbetter, J. R. (2020). Bacterial chemolithoautotrophy via manganese oxidation. *Nature*,
665 583(7816), 453–458. <https://doi.org/10.1038/s41586-020-2468-5>
- 666 Zahoransky, T., Kaiser, K., & Mikutta, C. (2022). High manganese redox variability and manganate
667 predominance in temperate soil profiles as determined by X-ray absorption spectroscopy.
668 *Geochimica et Cosmochimica Acta*, 338, 229–249. <https://doi.org/10.1016/j.gca.2022.10.016>
- 669 Zhang, J., Lion, L. W., Nelson, Y. M., Shuler, M. L., & Ghiorse, W. C. (2002). Kinetics of Mn(II)
670 oxidation by *Leptothrix discophora* SS1. *Geochimica et Cosmochimica Acta*, 66(5), 773–781.
671 [https://doi.org/10.1016/S0016-7037\(01\)00808-0](https://doi.org/10.1016/S0016-7037(01)00808-0)
- 672



Journal Pre-proof

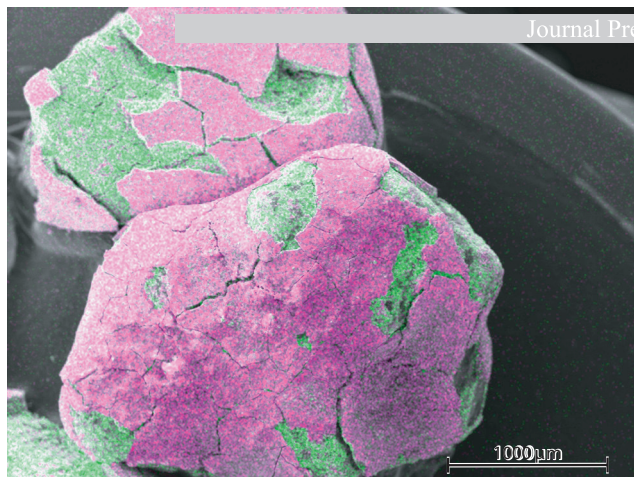




A)

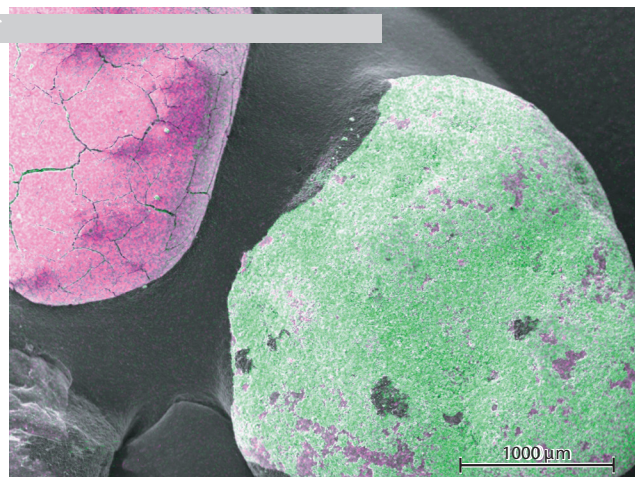
Before backwash

Top 5 cm

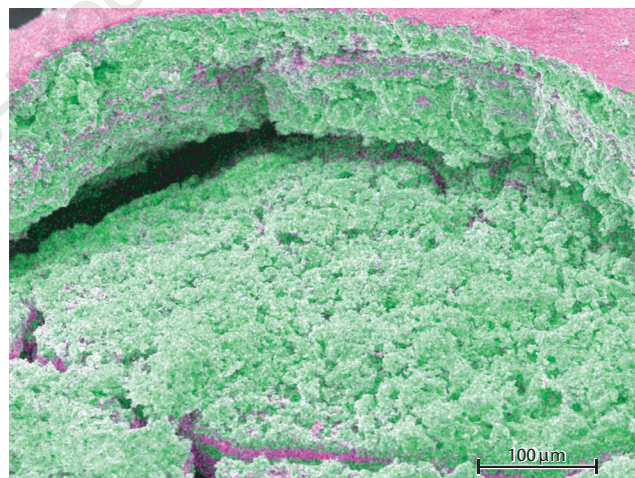
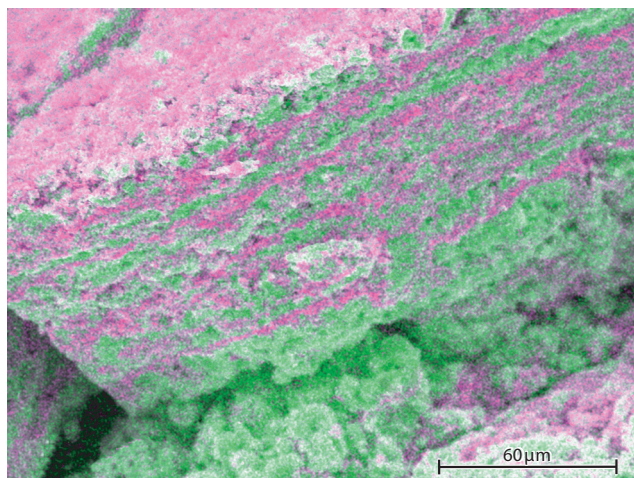


B)

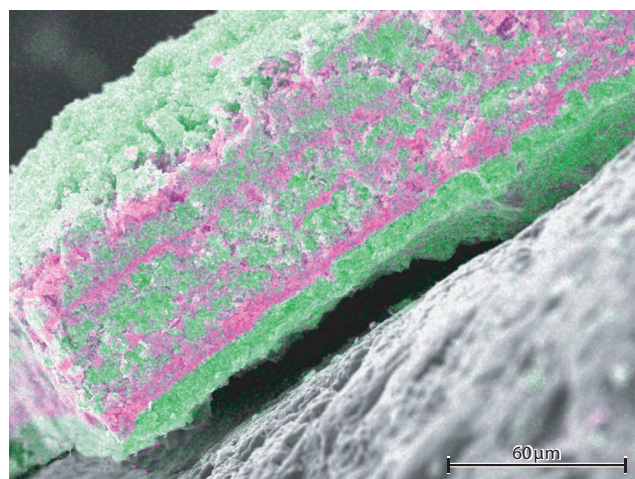
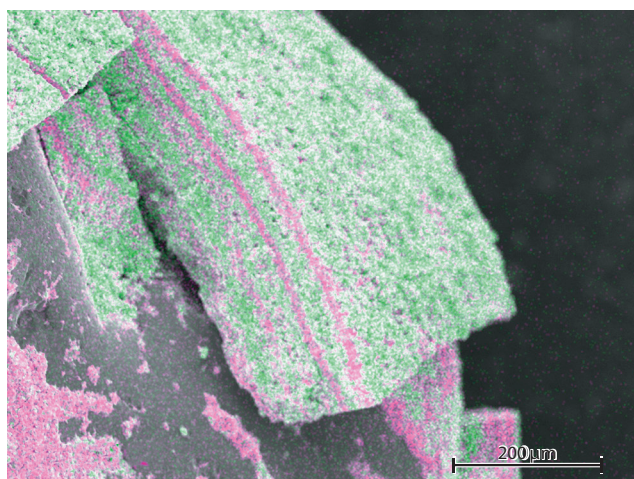
After backwash



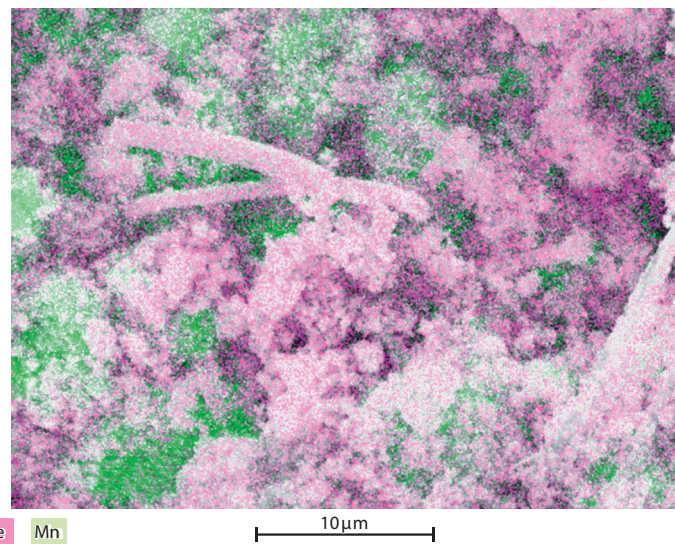
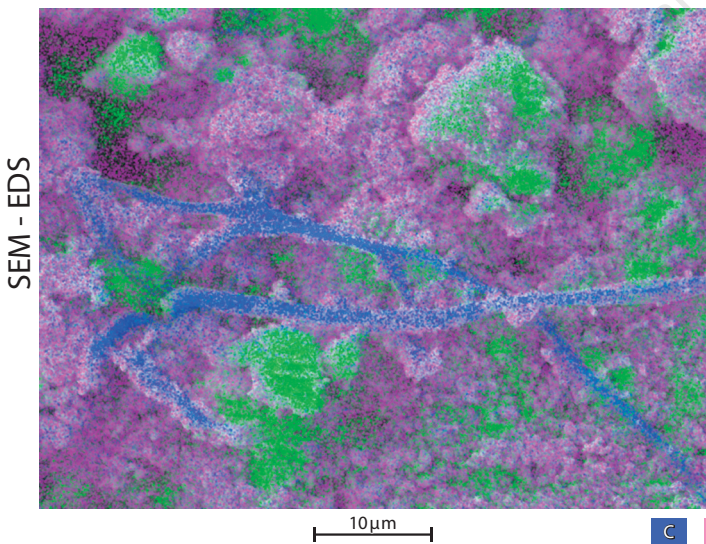
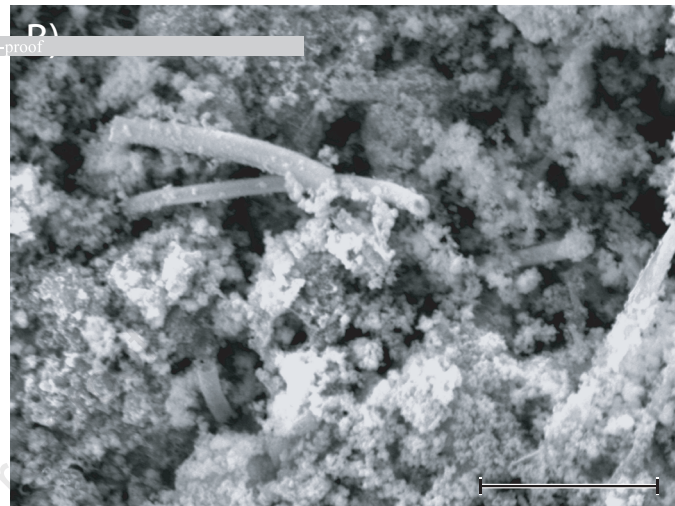
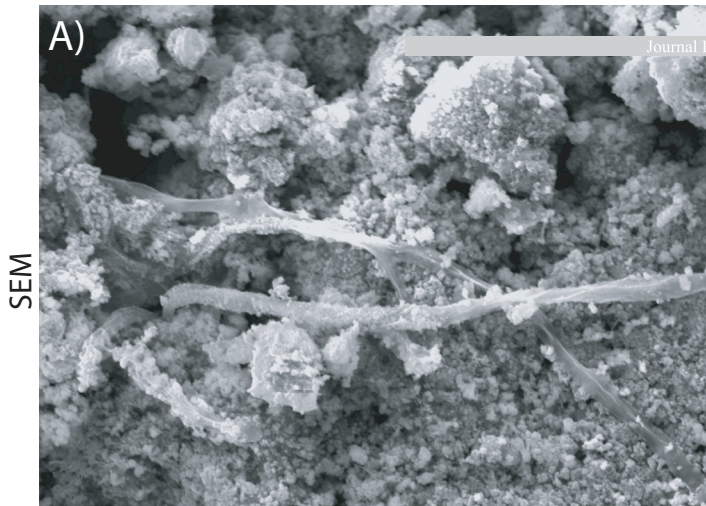
Top 5 cm



150 cm



Fe Mn

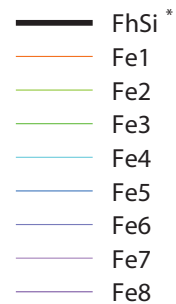
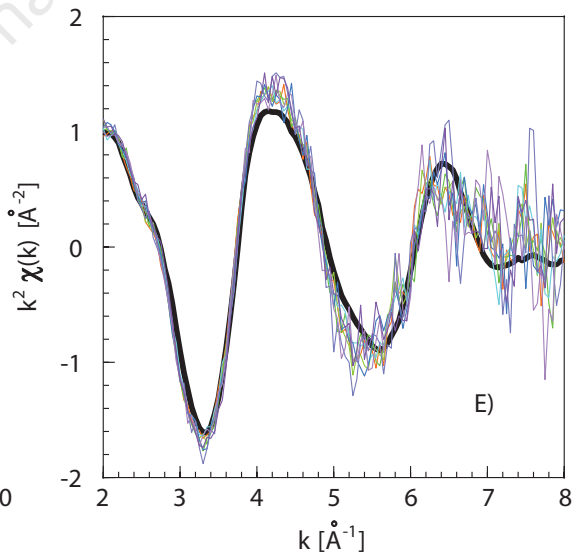
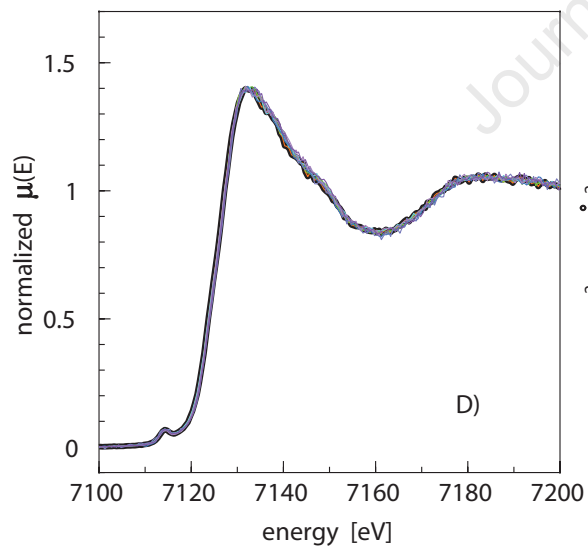
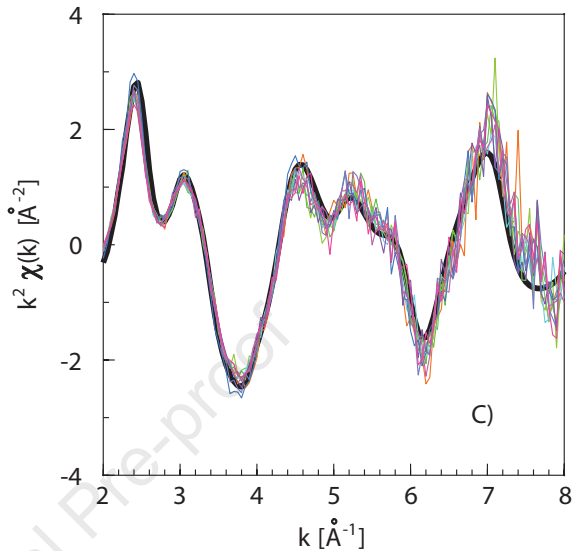
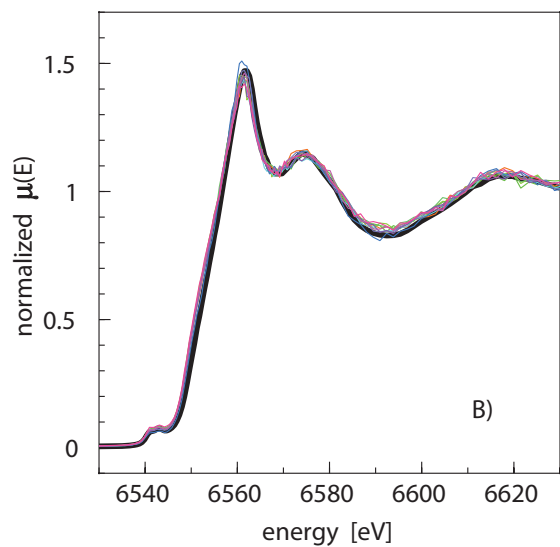


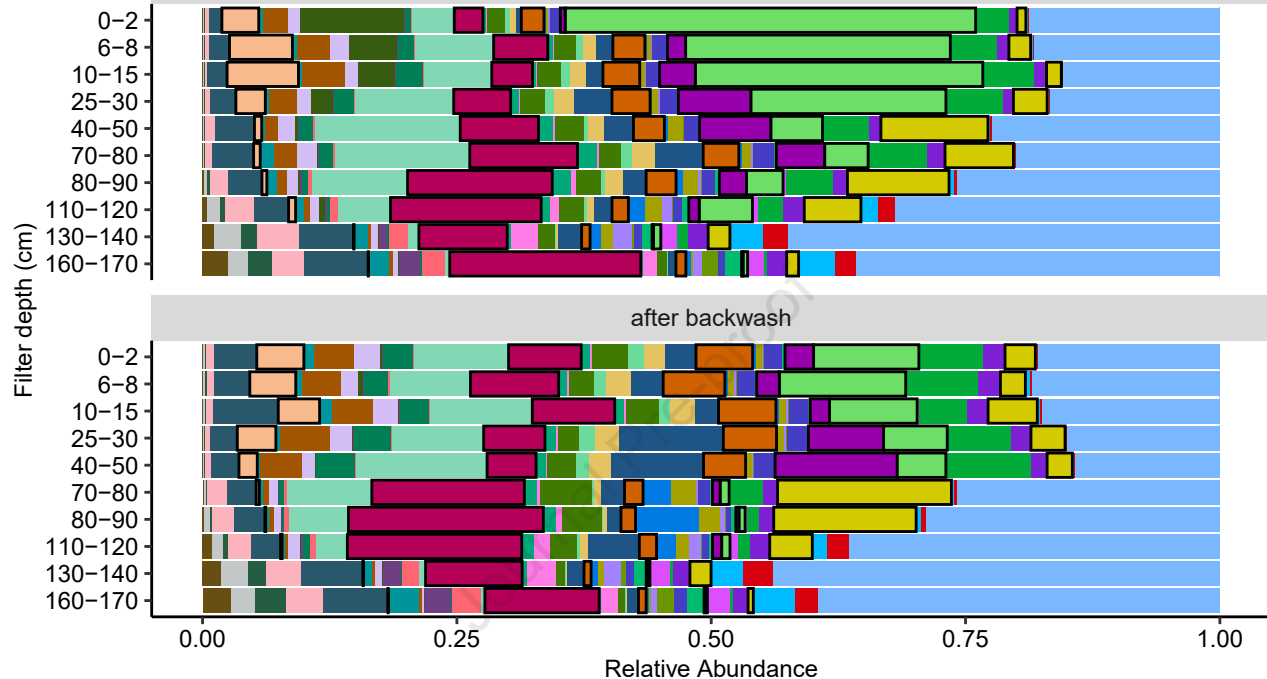
A)

100 μm 

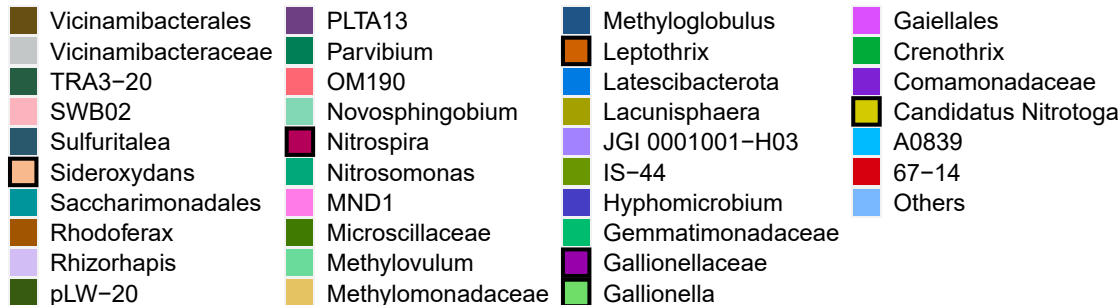
Fe7 Fe8

Mn7
Mn10Fe1 Fe6
Mn1 Mn6





Genus



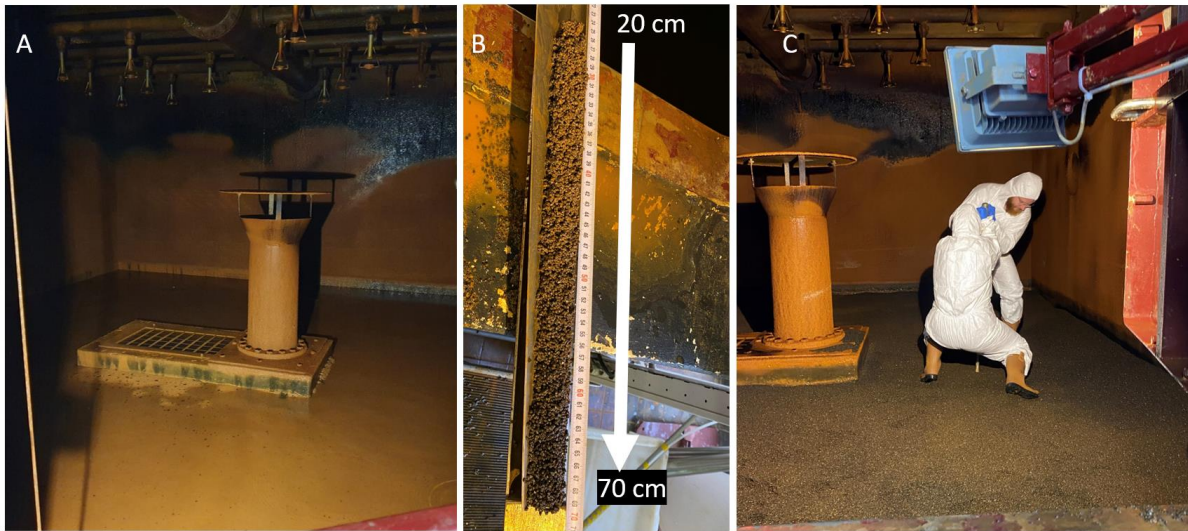


Figure 1. Photos taken during sampling of the filter in November 2021. A) Drained filter surface before backwash (74 h). B) Filter medium as collected from a depth of 20-70 cm in the filter before backwash showing a color transition from reddish-brown to blackish-brown. C) Drained filter surface after backwash, also showing people collecting filter medium.

Table 1. Concentrations of Fe, Mn and NH₄⁺ in rapid sand filters before (74 h) and after backwash (2h). Concentrations of total Fe, Mn, NH₄⁺, O₂, pH, and conductivity in the raw water (Raw), supernatant (Sn), at 50 cm depth in the filter, and in the effluent (Eff). For data from the additional sampling time points, see Supplementary Data.

Sample		Fe ²⁺ dissolved μM	Fe particulate μM	Mn dissolved μM	NH ₄ ⁺ μM	NO ₃ ⁻ μM	O ₂ μM	pH	Conductivity μS/cm
74 h	Raw	52	1	17	35	55	70	7.3	474
	Sn	5	47	17	35	55	280	7.4	471
	50 cm	0.5	0.1	8	12	74	218	7.3	462
	Eff	0.2	0	0	0.3	96	193	7.3	460
2 h	Raw	53	0	17	34	54	69	7.2	474
	Sn	45	7	17	34	55	280	7.4	471
	50 cm	2	0.5	7	11	73	233	7.4	463
	Eff	0.4	0.1	0	0.4	86	243	7.3	460

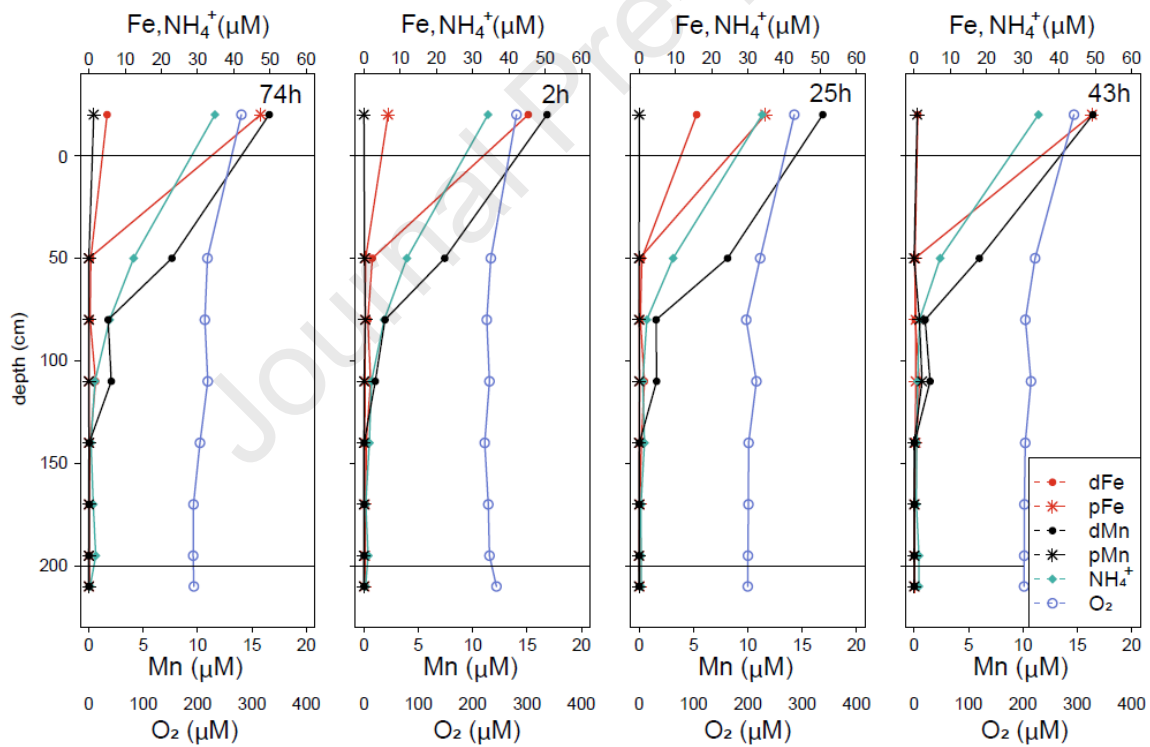


Figure 2. Depth profiles of Fe, Mn, NH₄⁺ and O₂ in the filter. A) 74 h runtime (just before backwash), B) 2 h, C) 25 h, and D) 44 h runtime after backwash. Dissolved Fe (dFe, red bullets), particulate Fe (pFe, red stars), dissolved Mn (dMn, black bullets), particulate Mn (pMn, black stars), NH₄⁺ (light green diamonds) and O₂ (purple hollow bullets), concentrations at different depths in the filter are shown.

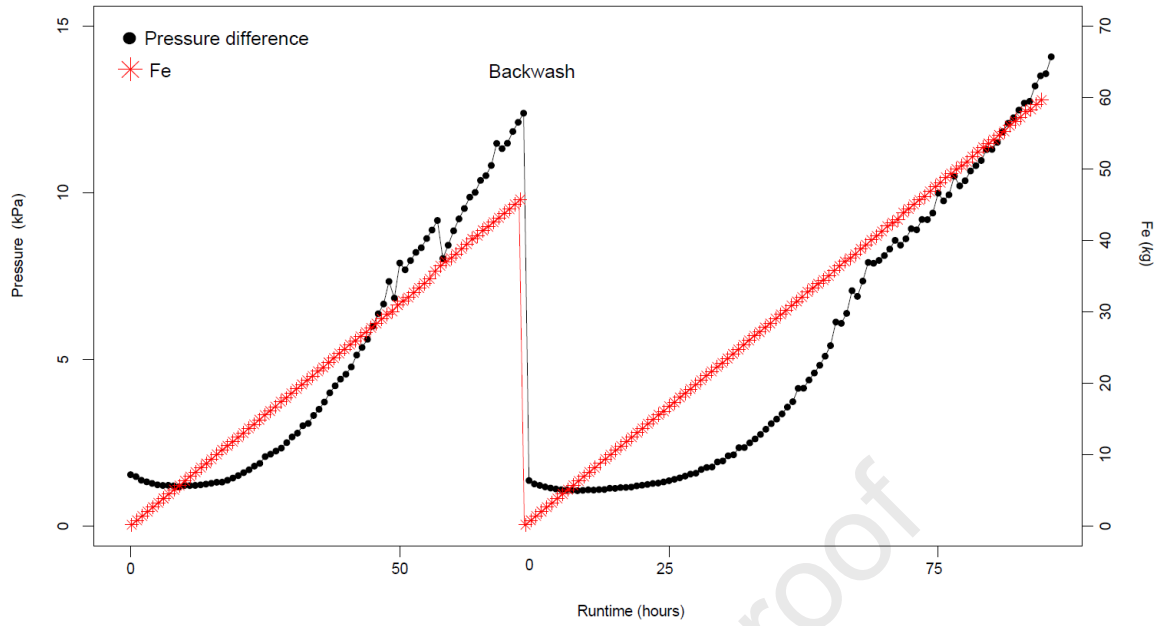


Figure 3. Pressure difference buildup in the filter as a function of filtration runtime in two backwash cycles. Pressure (black dots) and Fe load (red stars) over filter runtime are shown. The Fe load is estimated based on raw water concentrations (kg).

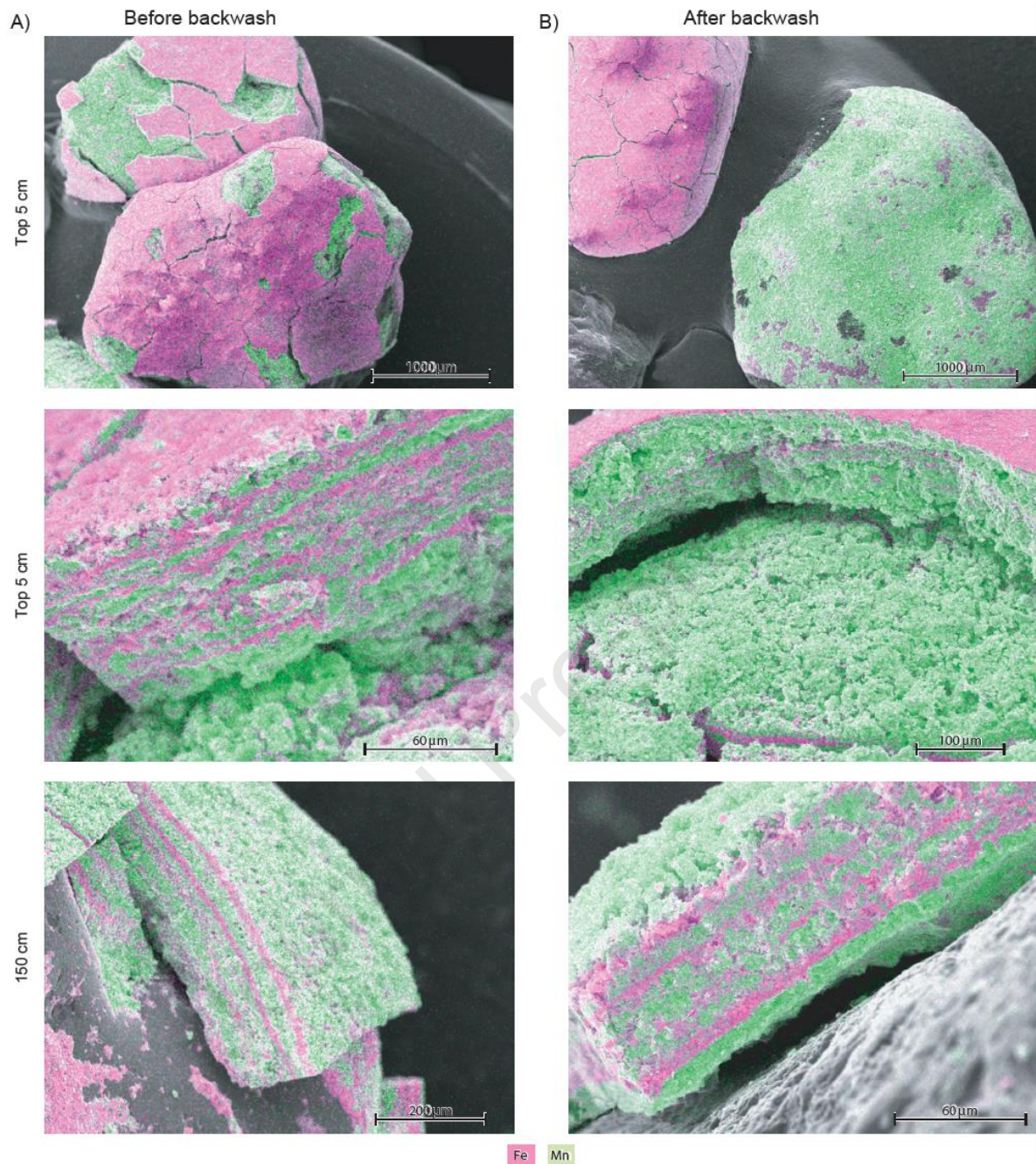


Figure 4. SEM-EDS images of filter medium coatings. A) before backwash (74 h) and B) after backwash (0 h). Samples were taken from the top (5 cm) and bottom (150 cm) of the filter. Fe is shown in pink, Mn in green.

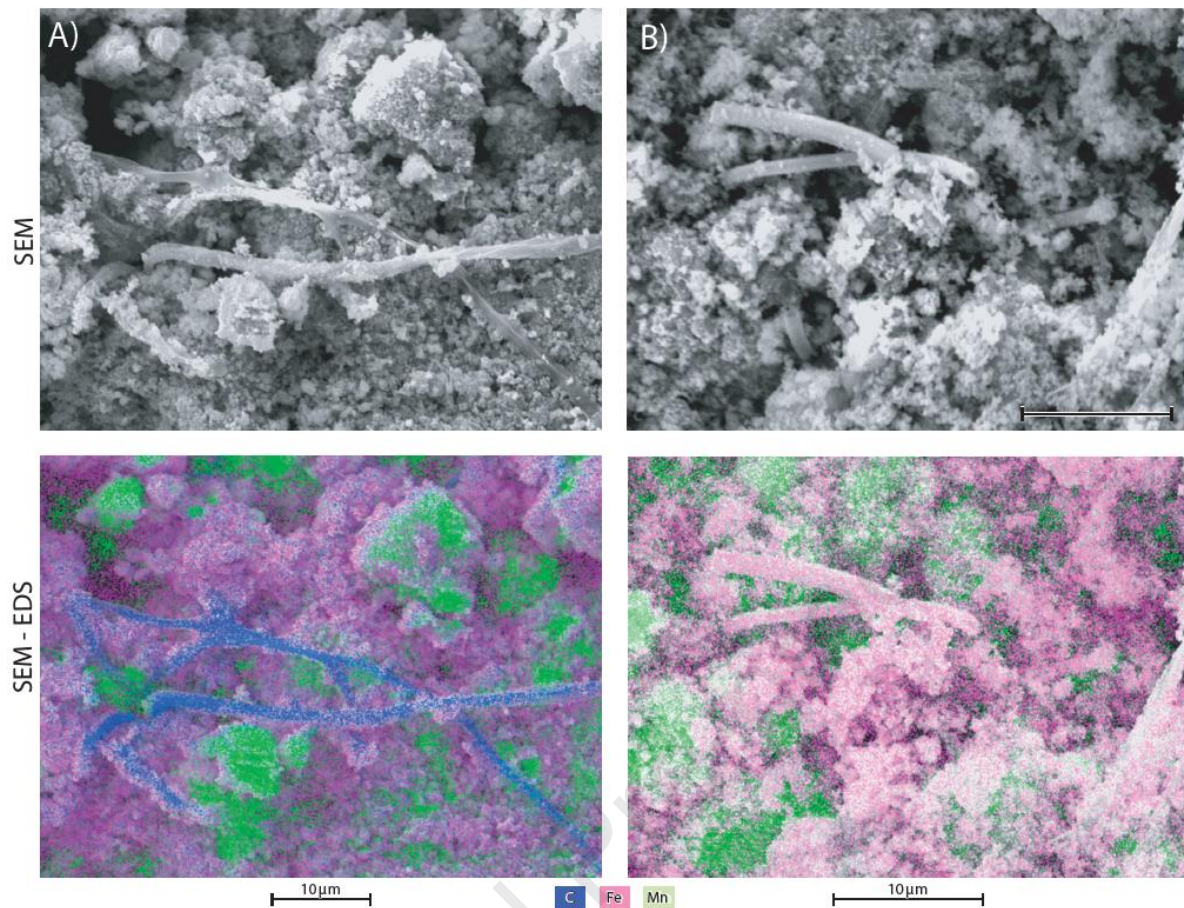


Figure 5. High resolution SEM and SEM-EDS images of microbial features on the filter medium. Sample was taken at 5 cm depth after backwash. A) Uncoated carbon-containing bacterial filaments and Mn-rich globular sponge-like structures; B) Fe-rich hollow sheets and Mn-rich globular sponge-like structures. Fe is indicated in pink, Mn in green and carbon (C) in blue.

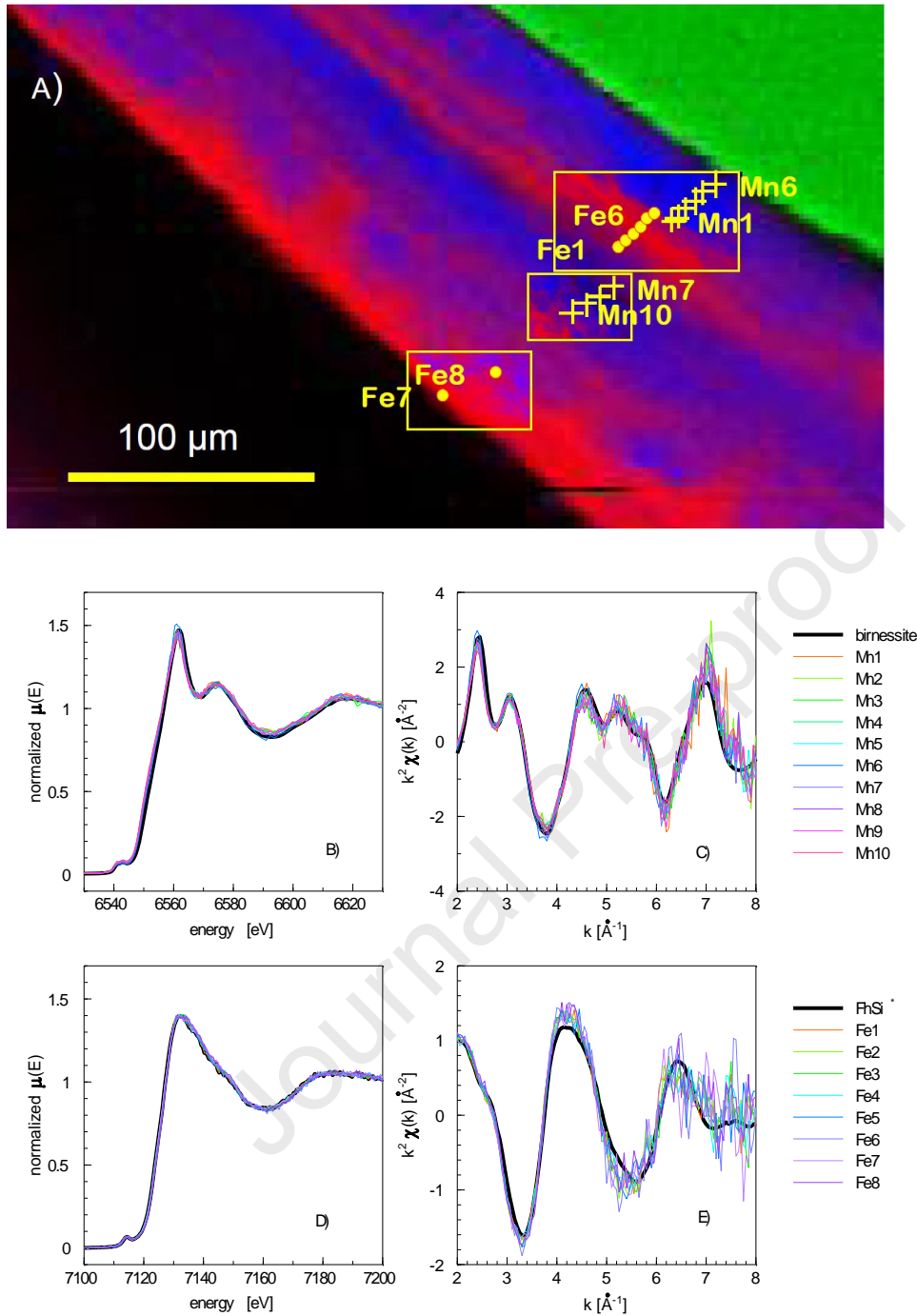


Figure 6. XAS-spectra indicating mineralogy and oxidation state between the alternating Fe and Mn-oxide layers in the coating A) Elemental map showing alternating Fe (red) and Mn (Blue) layers on a sand grain containing Si (green) and the locations on the coating for which X-ray absorption spectra for Fe (yellow dots) and Mn (yellow crosses) were obtained. The large map has been collected with a step size of 2 µm while the rectangles indicate area of interests mapped with a resolution of 0.5 µm. Self-absorption corrected B) Mn XANES and C) Mn EXAFS spectra for 10 locations on the coating and for microbial, hexagonal birnessite, and D) Fe XANES and E) Fe EXAFS for 8 locations on the coating and the Fe-Si* spectrum obtained from Senn et al. (2015).

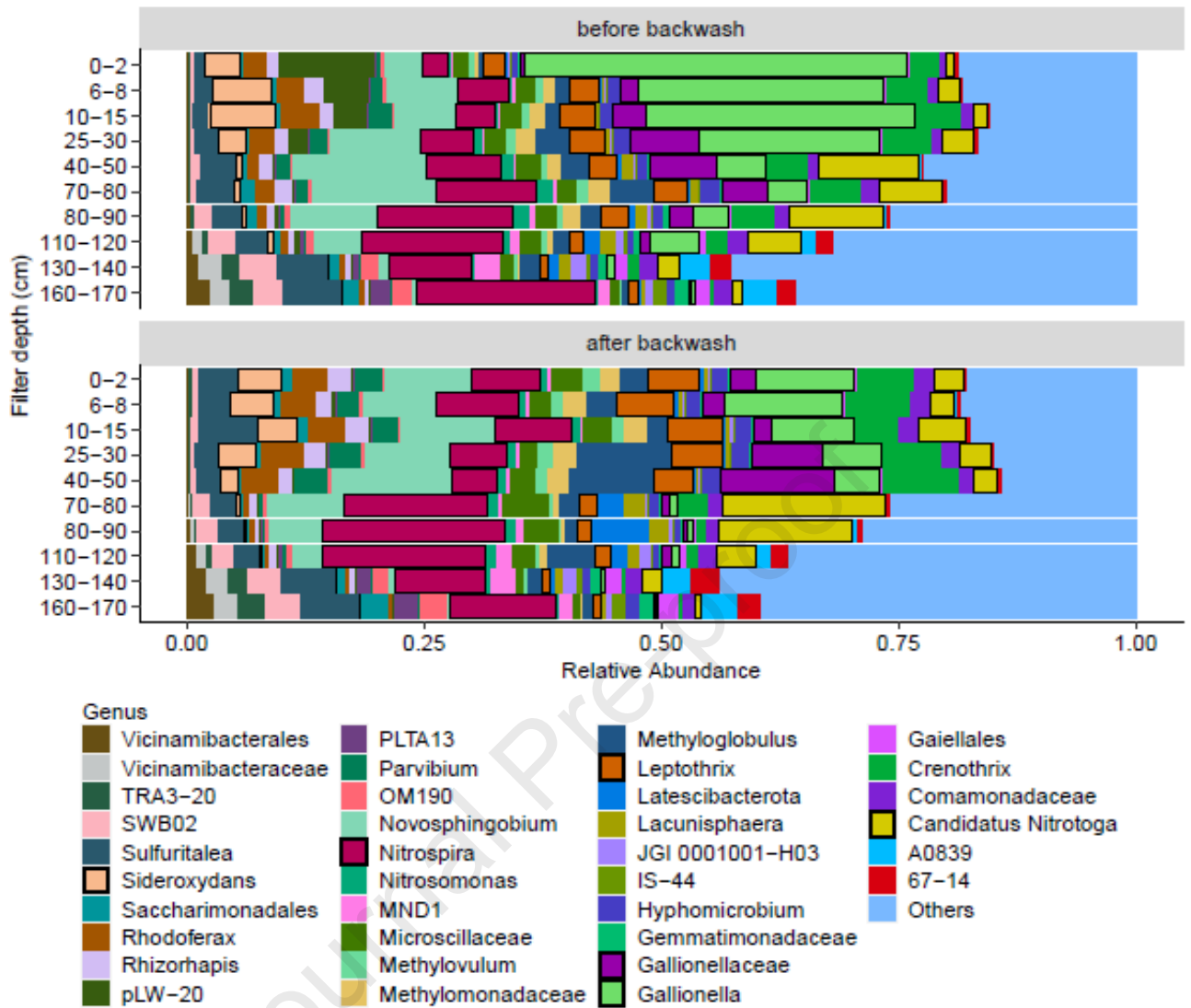


Figure 7. **Microbial community genus composition before and after backwash.** 16S rRNA gene amplicon sequencing-based relative microbial abundances A) before backwash B) and after backwash. *Sideroxydans*, *Nitrospira*, *Gallionella*, *Leptothrix* and *Candidatus Nitrotoga* are highlighted.

Highlights

- Fe removal occurs in the top of the filter while Mn is removed over a larger depth
- The microbial community remains stratified with depth after backwash
- *Gallionella*, *Leptothrix* and *Sideroxydans* are involved in Fe²⁺ oxidation
- Layered Fe and Mn-coatings throughout the filter suggest full mixing with time
- Backwash plays a crucial role in maintaining efficient water flow

Journal Pre-proof

Declaration of interests

The authors declare that they have no known competing financial interests or personal relationships that could have appeared to influence the work reported in this paper.

The authors declare the following financial interests/personal relationships which may be considered as potential competing interests:

Journal Pre-proof